EXPERIMENTAL INVESTIGATION OF THICK, AXIALLY SYMMETRIC BOUNDARY LAYERS ON CYLINDERS AT SUBSONIC AND HYPERSONIC SPEEDS

Thesis by

Ronald L. Richmond

In Partial Fulfillment of the Requirements

For the Degree of

Doctor of Philosophy

California Institute of Technology

Pasadena, California

1957

ACKNOWLEDGEMENTS

The author wishes to express his sincere appreciation for the extensive advice given by Dr. Donald Coles regarding this research project and to thank William M. Sublette for his excellent help in manufacturing the experimental models. Thanks are in order also to Professor Lester Lees for his comments on this report and to Mrs. Elizabeth Fox for her unequaled typing ability displayed herein.

ABSTRACT

An experimental investigation of the transverse curvature effect on laminar and turbulent axially symmetric boundary layers was conducted in two subsonic wind tunnels and in the GALCIT 5 x 5 inch hypersonic wind tunnel.

Subsonic turbulent skin friction coefficients were estimated from velocity profiles with axial flow on a 0.024 inch diameter cylinder and a 1.00 inch diameter cylinder. A considerable increase over the flat plate skin friction coefficient at the same momentum thickness Reynolds number was found.

Hypersonic laminar and turbulent skin friction coefficients with axial flow on an insulated 0.250 inch diameter cylinder were measured by the floating element technique and indicated, respectively, several times, and 1.5 times the laminar and turbulent flat plate skin friction coefficients at the same momentum thickness Reynolds numbers. Turbulent skin friction coefficients were estimated from pitot profiles with axial flow on a 0.064 inch diameter cylinder and on a 0.024 inch diameter cylinder at $M_1 \approx 5.8$ and indicate double the value to be found for an insulated flat plate at the same momentum thickness Reynolds number.

TABLE OF CONTENTS

TABLE OF CONTENTS (Cont'd)

LIST OF TABLES

LIST OF FIGURES

LIST OF FIGURES (Cont'd)

LIST OF SYMBOLS

SYMBOLS	DESCRIPTION
C	constant found in equation 3
C_f	local skin friction coefficient
d	circular cylinder diameter = $2r_o$
f	boundary layer function found in equation 1 and reference 10
F	function found in equation 10
G	function found in equation 9
H	function found in equation 6
ℓ	length of a body in x flow direction
M	Mach number
M_1	free stream Mach number
P	local static pressure
P_o	tunnel reservoir pressure
P_o'	local stagnation pressure behind a normal shock
q	free stream dynamic pressure = $\frac{1}{2}\rho_1 u_1^2$
r	radial distance from circular cylinder axis
r_o	circular cylinder radius
R	free stream Reynolds number
T	local static temperature (absolute)
T_1	free stream static temperature
T_o	stagnation temperature
T_w	wall recovery temperature
u, U	local axial velocity
u_1, U_1	free stream velocity
u_τ, U_τ	turbulent boundary layer "friction velocity"

LIST OF SYMBOLS (Cont'd)

SYMBOL	DESCRIPTION
v	local radial velocity
x	axial dimension
y	radial or lateral distance from the surface of a cylinder or flat plate = $r-r_o$ for a cylinder

GREEK SYMBOLS

δ	boundary layer thickness
δ^*	boundary layer displacement thickness defined in Appendix B
μ_1	free stream coefficient of viscosity
μ_w	wall value of viscosity coefficient
ν	coefficient of kinematic viscosity = μ/ρ
Φ	function found in equation 3
Ψ	streamfunction
ρ	local density
ρ_1	free stream density
ρ_w	density of fluid at a wall
ρ_τ	turbulent boundary layer "friction density"
τ_w	wall value of shearing stress
θ	boundary layer momentum thickness defined in Appendix B

I. INTRODUCTION*

Laminar Incompressible Boundary Layer Theories

Seban and Bond (1) have numerically solved the non-linear laminar boundary layer equations for the region of a circular cylinder near the nose where the basic laminar flow parameter $\nu x/u_1 r_0^2$ is small. Their solution was later pointed out to be in error and subsequently corrected by Kelly (2). An error in skin friction coefficient resulted from small numerical mistakes. Another error pointed out by Kelly was due to a physically incoherent definition of displacement thickness. For a boundary layer on a cylinder subjected to axial flow, the definition of δ^* which physically corresponds to that on a flat plate is

$$\int_{r_0}^{\delta^*+r_0} \rho\, u_1 2\pi r dr = \int_{r_0}^{\delta+r_0} \rho (u_1-u) 2\pi r dr$$

or

$$(\delta^*+r_0)^2 - r_0^2 = 2\int_{r_0}^{\delta+r_0} (u_1-u)\, r dr$$

This definition of δ^* was used earlier by Moore (3).

Cooper and Tulin (4), upon linearizing the Prandtl boundary layer equations, obtained a series solution for the friction on a circular cylinder in terms of powers of $\nu x/u_1 r_0^2$ for small values of that parameter and in terms of inverse powers of $\ell n(4\nu x/c u_1 r_0^2)$ for large values of $\nu x/u_1 r_0^2$. Flows with non-steady motion and pressure gradient were also treated.

For values of the parameter $\nu x/u_1 r_0^2$ greater than 100

---

*This investigation was conducted as a thesis subject with partial support from the U.S. Army (Contract DA-04-495-Ord-19).

Glauert and Lighthill (5) have obtained a series solution for the skin friction on a circular cylinder in terms of inverse powers of $\ell n(4\nu x/u_1 r_0^2)$. In addition a Pohlhausen type solution was obtained for arbitrary $\nu x/u_1 r_0^2$ giving, however, too low a value of skin friction. A complete curve of skin friction versus $\nu x/u_1 r_0^2$ using the Seban-Bond-Kelly solution for $\nu x/u_1 r_0^2$ less than 0.04, the Pohlhausen solution plus an arbitrary 9 percent for the range $0.04 < \nu x/u_1 r_0^2 < 100$, and the series solution for $\nu x/u_1 r_0^2$ greater than 100 was presented.

For $\nu x/u_1 r_0^2$ approaching infinity Stewartson (6) has also solved for the skin friction on a circular cylinder in terms of inverse powers of $\ell n(4\nu x/Cu_1 r_0^2)$ with the object of investigating laminar separation. The qualitative conclusion reached was that a thick, axially symmetric laminar boundary layer on a cylinder tends to delay separation.

Mark (7) has attempted to bridge the gap in $\nu x/u_1 r_0^2$ between the Stewartson result and the Seban-Bond-Kelly result by using assumed velocity profiles in von Karman's momentum integral relationship. Mark's approximation gave a lower value of laminar skin friction than either of the more exact analyses.

The primary qualitative result of all the above analyses is that the skin friction coefficient for an external axially symmetric laminar boundary layer on a cylinder is greater than that on a flat plate for similar boundary layer thicknesses. Glauert and Lighthill very aptly point out that fluid acceleration in the boundary layer near the solid boundary is small. This results in the

requirement that the shear force on succeeding cylindrical fluid surfaces near the cylinder wall be the same (i.e. $2\pi r\tau$ is approximately constant near the wall). Therefore, near the wall, the shear stress τ and hence $\partial u/\partial r$ vary like $1/r$ and thus indicate a larger value of skin friction than would exist on a comparable flat plate.

Laminar Compressible Boundary Layer Theories

Mark (7), as in the subsonic case, has used assumed velocity profiles in von Karman's momentum integral relation to obtain $C_f\sqrt{R_x}$ as a function of $u_1 r_0^2/4\nu_1 x$ with Mach number as a parameter. He shows that at $M_1 = 5.8$ for $u_1 r_0^2/4\nu_1 x > 10^5$, essentially the flat plate solution is obtained.

Probstein and Elliott (8) generalized Mangler's transformation to obtain simpler boundary layer equations in the two regions $\delta^*/r_0 >> 1$ and $\delta^*/r_o \lesssim 1$. In the latter region the first order correction to Mangler's solution for a circular cylinder was obtained by numerical integration.

The above two papers show that the transverse curvature has a greater effect on laminar skin friction, the higher the Mach number. Probstein and Elliott show that the transverse curvature term in the momentum and energy equations behaves as would a favorable pressure gradient, readily explaining an increase in skin friction and heat transfer coefficient and a delay in transition and separation. This term does not, however, significantly change the temperature recovery factor.

Turbulent Boundary Layer Theories

Eckert (9) has attempted to determine the effect of lateral curvature on turbulent skin friction when the boundary layer thickness δ becomes as large as the cylinder radius. After many simplifying assumptions it was found that when $\delta/r_0 = 1$, the incompressible local turbulent skin friction coefficient is 6 percent greater than that on a flat plate at the same Reynolds number based on x. Similarly an 8.5 percent increase was found at Mach 10. He concludes that these values of skin friction are probably too low.

It is this author's opinion that the only reliable method of attack on the turbulent, axially symmetric boundary layer on a cylinder is by way of extensive experimentation, especially in view of the lack of basic knowledge of turbulent processes even on flat plates.

Recently an effort has been made by Coles (10, 11, 12, 13) to interpret various experimental investigations of turbulent boundary layer flow from the point of view of similarity laws. Of particular importance here is the "streamline hypothesis" as proposed by Coles (11).

II. THE STREAMLINE HYPOTHESIS

For subsonic turbulent boundary layer flow on a flat plate experiments indicate the existence of a universal function

$$u/u_\tau = f(yu_\tau/\nu) \tag{1}$$

which is independent of pressure gradient. The "friction velocity", u_τ, is defined by the expression

$$\tau_w = \rho u_\tau^2 \tag{2}$$

Coles (11) has shown that equation 1, when appropriately combined with the continuity equation, implies that u/u_τ is constant on mean streamlines. The assumption that this latter property is generally valid is the "streamline hypothesis".

To develop an expression comparable to (1) for supersonic turbulent boundary layer flow on a cylinder we will assume the "streamline hypothesis" in the form

$$u/u_\tau = \Phi(C\Psi) \tag{3}$$

where Φ is an arbitrary function, Ψ is the stream function, C is a constant to be evaluated later, and u_τ is a function only of x.

Consider the continuity equation for compressible flow in cylindrical coordinates

$$\frac{\partial}{\partial x}(\rho u) + \frac{1}{r}\frac{\partial}{\partial r}(\rho v r) = 0 \tag{4}$$

from which a stream function can be defined by

$$\rho u r = \frac{\partial \Psi}{\partial r}; \qquad \rho v r = -\frac{\partial \Psi}{\partial x} \tag{5}$$

Now if we invert the streamline hypothesis, equation 3 becomes

$$C\Psi = H(u/u_\tau) \tag{6}$$

which upon differentiation and insertion of equation 5 becomes

$$C\,\frac{1}{r}\,\frac{\partial \Psi}{\partial r} = C\rho u = \frac{1}{r}\,H'(u/u_\tau)\,\frac{1}{u_\tau}\,\frac{\partial u}{\partial r} \tag{7}$$

At a given value of x we can integrate equation 7 to obtain

$$\int_{r_o}^{r} u_\tau C \rho\, r\, dr = \int_{0}^{u/u_\tau} \frac{H'(u/u_\tau)}{u/u_\tau}\, d\,(u/u_\tau) \tag{8}$$

or

$$C\,u_\tau \int_{r_0}^{r} \rho\, r\, dr = G(u/u_\tau) \tag{9}$$

If we now invert the function G we have

$$\frac{u}{u_\tau} = F\left[C u_\tau \int_{r_0}^{r} \rho\, r\, dr\right] \tag{10}$$

Using the Newtonian shear stress relation at the wall,

$$\tau_w = \mu_w\,(du/dr)_w \tag{11}$$

equation 10 implies

$$\left(\frac{du}{dr}\right)_{r=r_0} = \frac{\tau_w}{\mu_w}$$

$$= u_\tau \left\{ F'\left[C u_\tau \int_{r_0}^{r} \rho r dr\right] C u_\tau \frac{d}{dr}\left[\int_{r_0}^{r} \rho r dr\right]\right\}_{r=r_0} \tag{12}$$

which reduces to

$$\frac{\tau_w}{\mu_w} = C\, u_\tau^2\, F'(0)\ [\rho_w r_0] \tag{13}$$

Since C and $F'(0)$ are both arbitrary constants we may, without loss of generality, set

$$F'(0) = 1 \tag{14}$$

and thus define

$$C = \frac{\tau_w}{\mu_w \rho_w u_\tau^2 r_0} \tag{15}$$

Therefore

$$\frac{u}{u_\tau} = F\left\{ \frac{\tau_w}{\mu_w \rho_w u_\tau r_0} \int_{r_0}^{r} \rho r\, dr \right\} \tag{16}$$

As of this point u_τ and F are undefined functions. In order to show the reduction of this relationship (equation 16) to the subsonic flat plate relationship (equation 1), it is convenient to define, following Coles (11),

$$\tau_w = \rho_\tau u_\tau^2 \tag{17}$$

where ρ_τ is a "friction density" to be determined empirically. Furthermore, it is necessary that

$$F = f \tag{18}$$

where f is the well known empirically defined function of equation 1. Thus equation 16 becomes

$$\frac{u}{u_\tau} = f\left\{ \frac{\rho_\tau u_\tau}{\mu_w \rho_w r_0} \int_{r_0}^{r} \rho r dr \right\} \tag{19}$$

That equation 19 reduces to the flat plate incompressible case can be shown by relaxing first the curvature restraint and then the compressibility restraint or vice versa.

To obtain the compressible flat plate similarity coordinates we can let r_0 approach infinity. Keeping in mind that we are only interested in the region $r \cong r_0$ as r_0 approaches infinity, we can let $r/r_0 = 1$ and $dr = dy$ where $y = r - r_0$; then

$$\frac{u}{u_\tau} = f\left[\frac{\rho_\tau u_\tau}{\mu_w \rho_w} \int_0^y \rho \, dy \right] \tag{20}$$

To reduce this further to the incompressible flat plate case we set $\rho = \rho_\tau = \rho_w$ = constant and obtain

$$\frac{u}{u_\tau} = f\left[y \frac{u_\tau}{\nu} \right] \tag{21}$$

where $\nu = \mu / \rho$.

To obtain the incompressible similarity coordinates for flow on a cylinder we can set $\rho = \rho_\tau = \rho_w$ = constant in equation 19 to yield

$$\frac{u}{u_\tau} = f\left[\frac{u_\tau}{\nu} \frac{r^2 - r_0^2}{2r_0} \right] \tag{22}$$

Putting $2r_0 = d$ and simplifying equation 22 we obtain

$$\frac{u}{u_\tau} = f\left[\left(\frac{y u_\tau}{\nu} \right) \left(1 + \frac{y}{d} \right) \right] \tag{23}$$

which clearly indicates the "stretching" of the coordinate yu_τ/ν in the case of axial incompressible flow on a cylinder. Note also that when d = infinity the flat plate coordinates are recovered.

In order to determine ρ_τ for a particular supersonic boundary layer, both a local direct measurement of shear (τ_w) and a velocity profile must be obtained. Upon transforming the velocity profile to the coordinates of equations 19 or 20, depending upon the particular situation, a value of ρ_τ/ρ_w can be obtained by fitting the transformed profile to the universal incompressible flat plate function f in the region near the wall. It has been found by Coles (11) that ρ_τ/ρ_w is a function only of free stream Mach number for supersonic turbulent boundary layers on insulated flat plates. It will be shown later in this report that ρ_τ/ρ_w for supersonic axial flow on a cylinder has the value found by Coles for a flat plate at the same Mach number.

III. EXPERIMENTAL MODELS, INSTRUMENTATION, AND TECHNIQUES

A. Subsonic Facilities

1) Merrill Wind Tunnel

A one-inch diameter aluminum tube 12 feet long was located along the geometrical flow axis of the low speed Merrill wind tunnel. The nose of the tube was located in the tunnel settling chamber at the screens and the aft end well within the tunnel test section as displayed in fig. 1. To survey the axial external flow on the cylinder a single traversing pitot mechanism was used which clamped onto the model, thereby eliminating discrepancies between pitot motion and model motion. At the lowest tunnel speed usable in keeping with the least count of the alcohol micro-manometer, the boundary layer was found to be turbulent. Therefore for subsequent runs only a relatively high tunnel speed was used to insure manometer accuracy. Thus turbulent boundary layer velocity profiles were obtained at 8, 9, and 10 feet from the nose of the cylinder with approximately 155 ft/sec test section free stream velocity. No measurement of boundary layer axial symmetry was made on this model.

2) Low Turbulence Tunnel

A 0.024 inch diameter spring steel wire was installed parallel to the flow in the Low Turbulence tunnel as shown in fig. 2. The model was approximately 27 feet long of which the last 14 feet were in the uniform pressure test section of the tunnel. The wire fore end was draped over a pulley outside the intake of the tunnel and loaded in tension to 63 pounds (140,000 lbs/in^2) in order to maintain as straight as possible the horizontal portion of the model.

At this tensile stress the sag at the middle of a 23 foot length of wire would be approximately 0.020 inches. Approximately four feet from the rear of the wire model a vertical strut was located to move the rear of the model up, down, and to each side. With this strut and a double pitot sliding on and rotating about the wire model the boundary layer was forced to be symmetrical at the x station to be surveyed. The surveying instrument was a hot wire 0.0001 inches in diameter and 0.015 inches in span. The hot wire support was hinged to the same vertical strut so that much variation in distance between the hot wire and the wire model was eliminated. The hot wire was calibrated for mean flow by observing the shedding frequency of vortices in flow normal to a standardized cylinder. This method of calibration is nearly the only one possible at very low tunnel speeds when manometers are useless, and also is excellent at the higher speeds attainable in the present facility.

In addition to the above mentioned equipment a 10 foot long 8 inch diameter stovepipe was at times used in an attempt to align the flow around the model. Various boundary layer tripping devices were used on or near the wire model including a clay centerbody on the model, a blunting rubber ring on the nose of the stovepipe, and a cross tunnel wire near the start of the test section. Laminar and turbulent boundary layers were distinguished by observing an oscilloscope trace of the hot wire output.

B. Hypersonic Facility

Several cylinder models were installed and surveyed with pitot tubes in the GALCIT 5 x 5 inch hypersonic wind tunnel.

Because of the long model length required for naturally turbulent boundary layers and the desirability of using small diameter models to attain appreciable curvature effects, all models were supported from both ends in tension. Since a forward support in the supersonic tunnel flow would cause shock waves and a wake which might upset the boundary layer flow on the model, the forward support was located in the subsonic flow upstream of the tunnel throat. Therefore the models extended through the tunnel throat and their effect on the free stream flow had to be determined.

The three models shown in fig. 3 were used to determine the effect of their extension through the tunnel throat. Model 1 was 0.0625 inches in diameter for its entire length. Model 2 was 0.0625 inches in diameter through the throat and non-uniform supersonic expansion region and 0.250 inches in the test rhombus. The expansion was accomplished by a 1.5° half angle cone faired into the 0.250 inch size. Model 3 was 0.250 inches in diameter for its entire length except for notches at the tunnel throat. Free stream surveys were accomplished by an axially-traversing seven tube rake shown in fig. 3; the results are discussed in Section B1 of Part IV.

After determining the "model through the throat effect" a more detailed total head survey was made on the three models shown in fig. 4. Models 4 and 5 were 0.024 inches and 0.064 inches in diameter for their entire length. Model 6 was the same as model 2 except that a 3° half angle cone-ogive was used to reach the 0.250 inch size. Surveys were made axially and vertically with the 12

tube rake shown in fig. 4. Three tubes were located in each of four planes 90° apart around the models. The rear of each of the three cylinder models could be moved up and down from outside the tunnel while in operation, thus providing a means of making the boundary layer more symmetrical.

It was undertaken to construct a skin friction measuring device within a 0.250 inch cylinder. A first attempt was made by supporting a one-half inch long segment of the cylinder surface with split lock-washer type flexures and restraining it longitudinally with 0.0004 inch constantan strain wires at each end. This balance was marginal for sensitivity, was greatly affected by temperature gradients along the model, and proved wholly unsuccessful on tunnel starting due to the fragility of the strain wires.

A second, quite successful skin friction floating element balance was built within the 0.250 inch diameter segment of model number 7 shown in fig. 5. Externally, the floating element appeared as a 1/2 inch long segment of the 0.250 inch cylinder and was bounded by two 0.0025 inch gaps. As shown in fig. 5, a sliding shield with four pitot tubes attached was provided to protect the floating element on tunnel starting, to obtain zero force readings while the tunnel was hot and running, and to measure the axial symmetry of the boundary layer near the element station. The internal structure of the balance is shown in fig. 6. In order to support the entire model in tension a large structural member was required underneath the floating element. In the process of assembly this structural body was eventually pinned fore and aft

to the two segments of 0.250 inch stainless steel tubing. The floating element itself had a 0.005 inch thick wall. The floating components of the balance were located with respect to the fixed components by two split lock-washer type flexures shown in fig. 6. The flexures provided a quite rigid lateral support and an axial restraining spring force for the floating element. The spring force allowed a 0.001 inch longitudinal displacement of the element for a shear force of 500 milligrams. The floating element displacement was measured by determining the position of a magnetically conducting core within a transducer. The transducer was a center-tapped inductance coil wound on a thin stainless steel form and was excited by a 3 volt 31 kilocycle/second alternating-current voltage. In principle the inductance coil can be used as two legs of an alternating-current bridge, the other two being provided by a double resistance (potentiometer). Due to mis-matching of the bridge elements and internal capacitance to ground of the alternating-current instruments, it was found that a low enough A.C. null voltage to provide sufficient instrument sensitivity (least count) was unattainable. Therefore the electronic circuit of fig. 7 was developed. Essentially the small A.C. voltage was rectified and the resulting D.C. voltage read on a Leeds and Northrop potentiometer.

To calibrate the floating element a jewelled pulley was constructed whose support was clamped onto the 0.250 inch cylinder aft of the element. A single nylon fibre was attached to the floating element with hot wax, then draped over the pulley and loaded with a small pan and milligram weights. The break-out

force at the rim of the pulley was 3/4 milligram, a value quite small compared to the total of 500 milligrams applied during calibration. A typical calibration curve is shown in fig. 8. All calibrations resulted in a straight line which could be shifted horizontally to any desired position by the potentiometer R_5 shown in fig. 7.

IV. EXPERIMENTAL RESULTS

A. Subsonic Flow

1) Merrill Wind Tunnel

Turbulent boundary layer profiles were obtained from pitot surveys at three x stations on the one inch diameter cylinder. The data are presented in Table 1. The velocity profile at 9 feet is presented in fig. 9a in the usual coordinates and the one at 10 feet in the universal coordinates in fig. 9b. A turbulent skin friction coefficient can be estimated from fig. 9b with the aid of the streamline hypothesis as described in Appendix A. The computation of momentum thickness is described in Appendix B.

2) Low Turbulence Tunnel

Turbulent boundary layer profiles were obtained on the 0.024 inch diameter cylinder 16 feet from the tunnel screens. Varying the boundary layer tripping mechanism resulted in only slight differences in the momentum thicknesses and estimated friction coefficients. Typical data are presented in Table 2. The profile obtained with a clay centerbody trip and flow aligning stovepipe is presented in two sets of coordinates in figs. 10a and 10b. All attempts to obtain a steady laminar boundary layer on the model proved futile. At very low tunnel speeds the boundary layer on the cylinder appeared to be laminar and stable (with respect to transition) but was quite non-steady with respect to position about the model. The boundary layer axial non-symmetry was found to be continually changing in an unpredictable manner.

A summary of properties of the subsonic experimental turbulent boundary layer is found in Table 3 and in figs. 11 and

12. To extend the results to negative curvature effects, Laufer's (reference 14) pipe flow results are included. In fig. 12 the estimated turbulent skin friction due to axial flow on (or in) a cylinder is compared to the flat plate value of Coles (10), the comparison always being taken at the same momentum thickness Reynolds number.

B. Hypersonic Flow

1) Effect of Models Extending Through the Tunnel Throat

A rake survey showed no noticeable effect on the test rhombus free stream flow when a long 0.0625 inch cylinder extended through the flow expansion region and tunnel throat. Similarly, the free stream flow was unaffected by the composite 0.0625 and 0.250 inch model except for the very weak shock wave generated by the model conical expansion. The 0.250 inch cylinder contoured to fit the tunnel throat, however, seriously distorted the test rhombus flow and therefore was not tested further.

2) Alignment of the Models and Pitot Surveys

Complete axial surveys were made with the 12 pitot rake on the 0.024 inch, 0.064 inch, and on the composite 0.0625 and 0.250 inch cylinder. On all models the side boundary layer thicknesses were smaller than the top and bottom thicknesses. This effect was most pronounced at x = 10 to 12 inches from the tunnel throat where the tunnel side-wall throat waves cross the model.* Downstream of this point the axial symmetry steadily improved and was quite good at 24 inches. However, due to the presence of weak free stream waves at x = 24 inches, the final pitot surveys

---

*For further discussion of the throat waves see p. 98 of Ref. 16.

were obtained at x = 20 inches where the boundary layer was nearly symmetrical. A correction factor of from 0.842 to 0.866, depending on the free stream Reynolds number per inch, was applied to the momentum and displacement thicknesses as computed from the thicker boundary layer on top of the models.

In the hypersonic facility laminar and naturally turbulent boundary layers were found on all models tested. Typical raw data for three model sizes are presented in Table 4. Boundary layer profile plots are presented in figs. 13 to 18b inclusive. Included on the plots are the wall slopes as determined from measured laminar and turbulent shear on the 0.250 inch model, and estimated turbulent shear on the 0.064 inch and 0.024 inch models. The method of estimating turbulent skin friction from velocity profiles is described in Appendix A. The data reduction methods are described in Appendix C.

The computed Reynolds number based on average momentum thickness around the 0.250 inch cylinder at x = 20 inches is presented in fig. 19 for various tunnel reservoir pressures. It is believed that the computed point at $P_0 = 24.4$ lbs/in^2 is in error due to difficulty in estimating the free stream properties from the measured pitot profile; at this tunnel pressure the free stream pitot pressure at the outer edge of the boundary layer was not uniform, as evidenced from the profile presented in Table 4. Therefore the estimated point represented by the broken circle was used in all subsequent charts and tables. Further discussion can be found in Appendix B.

3) Measured Skin Friction on the 0.250 inch Cylinder

Fig. 20 is a plot of measured wall friction on the 0.250 inch model by use of the floating element balance located within the model 20 inches from the tunnel throat. It will be noted that laminar, transitional, and turbulent values were obtained. The repeatability of duplicate points taken on different days is seen to be excellent, being within $\pm$ 1.25 percent of the average. The dashpot contained air only, at a pressure equal to the floating element gap static pressure.

A summary of the measured laminar and turbulent skin friction on the 0.250 inch model and the estimated turbulent skin friction on the 0.064 and 0.024 inch models is presented in Table 5 and Table 6 and in fig. 21. Fig. 22 presents a comparison of laminar skin friction on a cylinder with the laminar flat plate value of Van Driest (reference 15) and turbulent skin friction on a cylinder with the turbulent flat plate value of Korkegi (reference 16). All comparisons were made at the same momentum thickness Reynolds number. Included in fig. 22 is the incompressible laminar theory of Glauert and Lighthill and an extension to compressible flow as described in Appendix D.

V. CONCLUSIONS

Steady, thick, subsonic axially symmetric laminar boundary layers on cylinders are difficult to obtain experimentally.

Steady, thick, supersonic axially symmetric laminar boundary layers are obtainable experimentally and indicate laminar skin friction several times that on a flat plate at the same Mach number and momentum thickness Reynolds number.

The skin friction associated with an axially symmetric subsonic turbulent boundary layer on a cylinder can be substantially greater than that on a flat plate at the same momentum thickness Reynolds number. The turbulent skin friction appears to approach an asymptotic value as θ/d, the transverse curvature parameter, becomes arbitrarily large.

At $M_1 = 5.8$, the skin friction due to an axially symmetric turbulent boundary layer on a cylinder can be double that for a flat plate at the same Mach number and momentum thickness Reynolds number.

The effect of transverse curvature on both laminar and turbulent skin friction is larger, the higher the free stream Mach number.

REFERENCES

1. Seban, R. A., and Bond, R., "Skin Friction and Heat Transfer Characteristics of a Laminar Boundary Layer on a Cylinder in Axial Incompressible Flow", J. Aero. Sci., V. 18, p. 671 (1951).

2. Kelly, H. R., "A Note on the Laminar Boundary Layer on a Circular Cylinder in Axial Incompressible Flow", J. Aero. Sci., V. 21, p. 634 (1954).

3. Moore, F. K., "Displacement Effect of a Three Dimensional Boundary Layer", N.A.C.A. TN 2722 (1952).

4. Cooper, R. D., and Tulin, M. P., The Laminar Flow About Very Slender Cylinders in Axial Motion, Including the Effect of Pressure Gradients and Unsteady Motions", D. W. Taylor Model Basin Rep. 838 (1953).

5. Glauert, M. B., and Lighthill, M. J., "The Axisymmetric Boundary Layer on a Long Thin Cylinder", Royal Soc. of London Proceedings, V. 230, p. 188 (1955).

6. Stewartson, K., "The Asymptotic Boundary Layer on a Circular Cylinder", Quart. Appl. Math., July 1955.

7. Mark, R. M., "Laminar Boundary Layers on Slender Bodies of Revolution in Axial Flow", GALCIT Hypersonic Wind Tunnel Memorandum No. 21 (1954).

8. Probstein, R. F., and Elliott, D., "The Transverse Curvature Effect in Compressible Axially Symmetric Laminar Boundary Layer Flow", J. Aero. Sci., V. 23, p. 208, March 1956.

9. Eckert, Hans U., "Simplified Treatment of the Turbulent Boundary Layer Along a Cylinder in Compressible Flow", J. Aero. Sci., V. 19, p. 23, (1952).

10. Coles, D., "The Problem of the Turbulent Boundary Layer", ZAMP, V 5, N 3, p. 181 (1954).

11. Coles, D., "The Law of the Wall in Turbulent Shear Flow", 50 Jahre Grenzshichtforschung (ed. by Görtler and Tollmien), F. Vieweg und Sohn, Braunschweig, p. 153 (1955).

12. Coles, D., "The Law of the Wake in the Turbulent Boundary Layer", J. of Fluid Mech., V. 1, Pt. 2, p. 191, July 1956.

13. Coles, D., "Remarks on the Equilibrium Turbulent Boundary Layer", GALCIT Miscellaneous Publication, June 1956.

14. Laufer, J., "The Structure of Turbulence in Fully Developed Pipe Flow", NACA TN 2954 (1953).

15. Van Driest, E. R., "The Laminar Boundary Layer with Variable Fluid Properties", Heat Transfer and Fluid Mechanics Institute, Univ. of Calif. at Berkeley, p. 127 (1954).

16. Korkegi, R. H., "Transition Studies and Skin Friction Measurements on an Insulated Flat Plate at a Mach Number of 5.8", J. Aero. Sci., V. 23, p. 97 (1956).

APPENDIX A

Estimation of Turbulent Skin Friction from a Velocity Profile

1) Subsonic Flow

Starting with the experimental boundary layer values of u and y near a cylinder model, a value of u_τ was determined which would cause the variables u/u_τ and $(yu_\tau/\nu)(1 + y/d)$ near the wall to fit the universal flat plate function given by Coles (10). From this value of u_τ the friction coefficient was computed according to

$$C_f = \frac{\tau_w}{q} = \frac{\rho u_\tau^2}{\frac{1}{2}\rho_1 u_1^2} = 2\left(\frac{u_\tau}{u_1}\right)^2$$

2) Hypersonic Flow

Starting with the experimental and computational values of ρ/ρ_w and r near the wall of a cylinder model evaluation at each data point of

$$\int_{r_0}^{r} \rho/\rho_w \, r\,dr$$

was made. It was assumed that $\rho_\tau/\rho_w = 1.74$ at $M_1 = 5.8$ (the flat plate value) for the cylinder. U_τ was estimated and the variables

$$u/u_\tau \quad \text{and} \quad \frac{\rho_\tau u_\tau}{\mu_w r_0} \int_{r_o}^{r} \frac{\rho}{\rho_w} \, r\,dr$$

plotted on the same universal subsonic flat plate curve of Coles (10). At times a re-estimation of u_τ was necessary. Note that μ_w and ρ_w, the wall values of viscosity coefficient and density, must be determined at the actual wall recovery temperature, and not at the free stream stagnation temperature. The local turbulent

skin friction coefficient was then computed from

$$C_f = \frac{\tau_w}{q} = \frac{\rho_\tau u_\tau^2}{\frac{1}{2}\rho_1 u_1^2} = 2\,\frac{\rho_\tau}{\rho_1}\,\left(\frac{u_\tau}{u_1}\right)^2$$

Invariably, values of u near a wall in a compressible boundary layer as determined from pitot pressures are too high. Therefore after estimating the wall shear and hence the wall slope of the velocity profile, a much more reasonable value of u was estimated from the relation

$$\tau_w = \mu_w\,(u/y) \text{ near the wall}$$

Such estimated velocities are represented by the doubly flagged circles in figs. 14b, 16b, and 18b.

APPENDIX B

Relationships for Determination of Displacement and Momentum Thicknesses

The boundary layer momentum thickness which physically corresponds to that on a flat plate is defined by

$$\int_{r_0}^{\theta+r_0} \rho_1 u_1^2 2\pi r dr = \int_{r_0}^{\delta+r_0} \rho u(u_1-u)\, 2\pi r dr$$

or

$$(\theta+r_0)^2 - r_0^2 = \int_{r_0^2}^{(\delta+r_0)^2} \frac{\rho u}{\rho_1 u_1}\left(1-\frac{u}{u_1}\right) d(r^2)$$

Similarly the displacement thickness is defined by

$$(\delta^*+r_0)^2 - r_0^2 = \int_{r_0^2}^{(\delta+r_0)^2} \left(1-\frac{\rho u}{\rho_1 u_1}\right) d(r^2)$$

The incompressible definitions can be obtained by merely setting $\rho/\rho_1 = 1$.

In the right hand integral of the above expressions the additional r appearing results in a greater contribution to mass or momentum defect from the outer regions of an axially symmetric boundary layer than would be obtained for a flat plate boundary layer. Therefore the computed values of δ^* and θ are greatly affected by the choice of free stream velocity and boundary layer thickness. In addition the choice of free stream velocity and boundary layer thickness is more difficult than for a flat plate due to the added fullness of the axially symmetric boundary layer velocity profile. This

problem is slightly lessened for the supersonic boundary layer if we choose the free stream quantities and boundary layer thickness from a Mach number profile rather than a velocity profile as may be evidenced from figs. 13 through 18.

APPENDIX C

Supersonic Boundary Layer

Flow Data Reduction Methods

The measured data included P_0 and T_0, the tunnel reservoir pressure and temperature, and a profile of y versus P_0', the pitot pressure in the boundary layer and free stream.

By assuming isentropic free stream tunnel flow the free stream Mach number was obtained and thus the free stream static pressure and temperature determined. By using Rayleigh's pitot formula and by assuming constant static pressure through the boundary layer a Mach number profile was obtained. Then assuming a constant T_0 through the boundary layer (i.e. an adiabatic relationship between M and T in the boundary layer) and the perfect gas law, density, temperature, and velocity profiles were obtained. Free stream Reynolds number per inch was computed by assuming Sutherland's viscosity law holds even at the low free stream temperatures obtained (90° Rankine).

For determination of the wall values of the flow variables assumed temperature recovery factors of 0.9 for the turbulent and 0.86 for the laminar boundary layer were employed. The wall viscosity was then determined from Sutherland's viscosity law

$$\mu_w = \frac{2.27 \times 10^{-8} T_w^{3/2}}{T_w + 198.6} \quad \text{lb sec/ft}^2$$

where T_w is in degrees Rankine. To determine the wall velocity slope or Mach number slope from the measured or estimated wall shear the following simple relations were used:

$$\tau_w = \mu_w \left(\frac{du}{dr}\right)_w$$

$$\left[\frac{dr}{d(u/u_1)}\right]_w = \frac{u_1}{(du/dr)_w}$$

$$\left[\frac{dr}{d(M/M_1)}\right]_w = \sqrt{\frac{T_w}{T_1}} \left[\frac{dr}{d(u/u_1)}\right]_w$$

APPENDIX D

Reduction of Laminar Theory to Local Properties

Inherent in all of the laminar theories of Part I of this paper is the quantity x. Since there is no definable x for the present experiments, comparison with theory can only be accomplished by elimination of x from them.

In principle, at least for most of the theories mentioned, the boundary layer momentum thickness, θ, can be found as a unique function of x, thus permitting evaluation of the friction coefficient, C_f, as a function only of the local property θ. Fortunately (for the present purpose) Glauert and Lighthill (5) have tabulated their results in such a way that discrete values of C_f and θ are immediately obtainable. The necessary transformations from the notation of reference 5 to the present notation are:

Ref. 5 Notation		Present Notation
$\frac{F}{\mu U}$	$\longrightarrow$	$\frac{\pi}{\theta/r_0} R_\theta C_f$
$\frac{\textcircled{H}}{\pi a^2}$	$\longrightarrow$	$(\frac{\theta}{r_0} + 1)^2 - 1$

The resulting curve of C_f/C_f (flat plate) versus θ/d for incompressible laminar flow is presented in fig. 22.

Coles, in a private communication, noted that a simple transformation of the compressible flow variables would allow extension of the incompressible Glauert-Lighthill solution to the compressible case. The transformation is

$$\rho\, r\, dr = \rho_w\, \bar{r}\, d\bar{r}$$

The new variable $\bar{r}$ can have limits similar to those for r if we choose an integration constant such that

$$\bar{r}^2 = r_0^2 + 2\int_{r_0}^{r} \frac{\rho}{\rho_w}\, r\, dr$$

The assumed velocity profile in the new variables is

$$\frac{u}{u_1} = \frac{\ell n\,(\bar{r}/r_0)}{a_c}$$

which is quite similar to that used by Mark (7), and reduces exactly to the Glauert-Lighthill profile for incompressible flow. It can easily be shown that the Glauert-Lighthill tabulated incompressible quantities have the same mutual relationships as the transformed quantities noted below.

Ref. 5 Incomp. Notation		Ref. 5 Comp. Notation		Present Comp. Notation
$\frac{F}{\mu U}$	$\longrightarrow$	$\frac{F}{\mu_w U}$	$\longrightarrow$	$\frac{\pi}{(\mu_w/\mu_1)(\theta/r_0)} C_f R_\theta$
$\frac{\Theta}{\pi a^2}$	$\longrightarrow$	$\frac{\Theta}{\pi a^2}$	$\longrightarrow$	$\frac{\rho_1}{\rho_w}\left[\left(\frac{\theta}{r_0}+1\right)^2 - 1\right]$
$\frac{\nu x}{Ua^2}$	$\longrightarrow$	$\frac{\nu_w x}{Ua^2}$	$\longrightarrow$	$\frac{\nu_w x}{u_1 r_0^2}$

The resulting C_f/C_f (flat plate) versus θ/d is plotted in fig. 22.

The following table is taken from Glauert-Lighthill with the above transformations included.

Incompressible			Compressible ($M_1 = 5.8$)		
θ/d	$C_f R_\theta$	$\frac{C_f}{C_f(\text{Flat Plate})}$	θ/d	$C_f R_\theta$	$\frac{C_f}{C_f(\text{Flat Plate})}$
.0108	.4864	1.012	.00141	.4913	1.021
.0190	.4938	1.028	.00249	.5003	1.040
.0350	.5470	1.13	.00467	.5647	1.18
.0648	.6390	1.33	.00884	.6743	1.40
.1199	.7633	1.59	.01708	.8405	1.75
.2240	.9868	2.05	.03432	1.169	2.43
.4151	1.324	2.76	.0709	1.749	3.64
.762	1.887	3.93	.1509	2.889	6.02
1.364	2.683	5.58	.3168	4.817	9.25
2.355	3.762	7.83	.628	7.756	16.1
4.036	5.369	11.2	1.197	12.31	25.6
7.33	8.305	17.3	2.677	23.45	48.8
11.5	11.35	23.6	4.343	33.13	69.0

In the above tabulation $R_\theta C_f$ (flat plate) was taken as the Blasius value, 0.4409, plus 9%.

An attempt was made to examine compressible laminar skin friction on a cylinder by deriving a velocity profile which would identically satisfy the energy equation, the transport terms in the momentum equation being neglected. The resulting $C_f R_\theta$ at particular θ/d values was considerably lower than that above.

Table 1

Merrill Wind Tunnel Turbulent Boundary Layer
Velocity Profile Data

Free stream velocity = u_1 = 154 ft/sec

Model diameter = 1.0 inches

Distance from tunnel screens = x

y (inches)	x = 8 feet u/u_1	x = 9 feet u/u_1	x = 10 feet u/u_1
0.02	.611	.581	.574
0.04	.691	.662	.661
0.06	.732	.694	.688
0.08	.759	.728	.725
0.10	.788	.755	.750
0.145	.821	.794	.793
0.19	.868	.833	.816
0.23	.887	.860	.844
0.27	.912	.885	.864
0.35	.949	.924	.902
0.44	.971	.949	.925
0.52	.984	.965	.952
0.69	.998	.984	.972
0.85	1.000	.998	.987
1.105	1.001	1.000	.998
1.27	1.000	1.000	.998
1.435	1.001	1.000	1.000
1.605	0.999	1.002	1.000

Table 2

Low Turbulence Tunnel Turbulent Boundary Layer
Velocity Profile Data

Model Diameter = 0.024 inches

Distance from Tunnel Screens = 16 feet

y (inches)	u (cm/sec)	y (inches)	u (cm/sec)	y (inches)	u (cm/sec)	y (inches)	u (cm/sec)
0.006	490	0.012	625	0.012	684	0.009	149
0.009	570	0.015	746	0.015	730	0.012	172
0.012	690	0.018	831	0.018	822	0.015	200
0.015	805	0.021	891	0.021	882	0.018	236
0.018	864			0.024	917	0.021	262
0.021	910	0.027	950	0.027	955	0.024	275
0.024	945					0.027	300
0.027	970	0.042	1020	0.033	994	0.030	313
0.030	988	0.057	1052				
		0.072	1065	0.042	1032	0.045	351
0.036	1023	0.087	1083	0.057	1075	0.060	376
0.042	1042	0.102	1096	0.072	1096	0.075	386
				0.087	1117	0.090	395
0.057	1070	0.132	1110				
0.072	1091	0.147	1118	0.117	1139	0.120	409
0.087	1107						
0.102	1119	0.177	1122	0.162	1162	0.165	420
		0.207	1139	0.237	1183	0.240	430
0.177	1145			0.312	1201	0.315	439
0.252	1160	0.252	1151				
0.327	1173			0.462	1219	0.465	440
		0.327	1161	0.612	1230	0.615	448
0.477	1191	0.477	1182	0.762	1232	0.765	455
0.627	1209	0.627	1196	0.912	1238	0.915	459
0.777	1220	0.777	1201	1.062	1239	1.065	459
0.927	1230	0.927	1211				
1.077	1240	1.077	1219				
Natural Transition		Clay Centerbody Trip		Clay Centerbody Trip and Stovepipe		Clay Centerbody Trip and Stovepipe	

Table 3

Summary of Subsonic Turbulent Boundary Layer Curvature Effects

M_1	d (inches)	δ^* (inches)	θ (inches)	θ/d	R_θ	C_f	C_f/C_f'(flat plate)	Reference
0.089	9.72		-0.268	-0.0276	13,750	0.00247	1.037	Laufer Pipe (Ref. 14) Friction by Pressure Drop
0.1375	1.00	0.085	0.069	0.069	5,540	0.00323	1.15	Merrill Wind Tunnel Estimated Skin Friction
	1.00	0.109	0.094	0.094	7,540	0.00305	1.15	
	1.00	0.125	0.109	0.109	8,750	0.00290	1.13	
0.036	0.024	0.123	0.0995	4.15	2,100	0.00495	1.47	Low Turbulence Tunnel Estimated Skin Friction
	0.024	0.140	0.135	5.6	2,800	0.00518	1.61	
	0.024	0.162	0.156	6.5	3,310	0.00518	1.67	
0.014	0.024	0.109	0.122	5.1	954	0.00592	1.50	

/ C_f(flat plate) due to Coles (Ref. 10)

δ^* and θ are defined in Appendix B

Table 4

Hypersonic Boundary Layer Profile Data

Distance from Tunnel Throat = 20 inches

Model Diameter = 0.024 inches

Turbulent		Laminar	
r (inches)	M	r (inches)	M
0.017	1.72	0.017	1.48
0.035	2.79	0.035	1.81
0.053	3.72	0.053	2.24
0.072	4.04	0.072	2.52
0.090	4.27	0.090	2.76
0.108	4.49	0.108	3.02
0.144	4.84	0.126	3.21
0.180	5.14	0.144	3.51
0.217	5.41	0.163	3.78
0.254	5.62	0.181	4.11
0.290	5.73	0.199	4.47
0.331	5.78	0.217	4.81
0.372	5.79	0.235	5.10
0.408	5.80	0.254	5.31
0.445	5.82	0.272	5.43
0.481	5.82	0.290	5.51
0.517	5.83	0.308	5.54
0.554	5.83	0.333	5.58
0.572	5.83	0.357	5.33
P_0 = 84.35 psia		P_0 = 24.4 psia	
T_0 = 225° F		T_0 = 225° F	

Table 4 (Cont'd)

Model Diameter = 0.064 inches

Turbulent		Laminar	
r (inches)	M	r (inches)	M
0.037	0.92	0.037	1.02
0.046	1.31	0.055	1.02
0.055	2.31	0.073	1.13
0.064	2.88	0.092	1.44
0.073	3.19	0.110	1.99
0.092	3.51	0.128	2.61
0.110	3.79	0.146	3.36
0.128	4.01	0.164	4.08
0.164	4.36	0.183	4.59
0.201	4.66	0.201	4.95
0.237	4.92	0.219	5.15
0.274	5.14	0.237	5.29
0.310	5.32	0.255	5.47
0.335	5.41	0.274	5.62
0.359	5.50	0.292	5.72
0.396	5.63	0.310	5.75
0.432	5.74	0.336	5.75
0.468	5.78	0.363	5.74
0.505	5.79	0.381	5.74
0.541	5.79	0.399	5.74
0.559	5.79	0.417	5.74
P_0 = 84.4 psia		P_0 = 24.4 psia	
T_0 = 225° F		T_0 = 225° F	

Table 4 (Cont'd)

Model Diameter = 0.250 inches

Turbulent				Laminar			
r (inches)	M	r (inches)	M	r (inches)	M	r (inches)	M
0.130	1.12	0.130	0.91	0.130	0.96	0.130	1.27
0.142	1.41	0.142	1.10	0.157	1.12	0.152	1.31
0.152	1.97	0.152	1.95	0.182	1.24	0.177	1.35
0.162	2.48	0.162	2.45	0.207	1.43	0.202	1.50
0.172	2.82	0.172	2.80	0.232	1.67	0.227	1.64
0.182	3.02	0.182	3.03	0.257	2.03	0.252	1.89
0.207	3.41	0.207	3.42	0.282	2.61	0.277	2.20
0.232	3.73	0.232	3.67	0.295	2.97	0.302	2.48
0.257	3.99	0.257	4.01	0.307	3.39	0.327	2.92
0.282	4.26	0.282	4.29	0.320	3.90	0.352	3.54
0.307	4.52	0.307	4.57	0.332	4.33	0.377	4.31
0.332	4.76	0.332	4.84	0.345	4.64	0.402	4.84
0.357	5.05	0.357	5.10	0.357	4.83	0.427	5.09
0.382	5.24	0.382	5.32	0.370	4.96	0.477	5.40
0.407	5.44	0.407	5.49	0.382	5.06	0.527	5.53
0.432	5.60	0.432	5.61	0.407	5.19	0.577	5.54
0.457	5.68	0.457	5.68	0.432	5.35	0.627	5.60
0.482	5.73	0.482	5.73	0.457	5.43		
0.507	5.77	0.507	5.75	0.482	5.51		
0.532	5.77	0.532	5.75	0.507	5.58		
0.557	5.78	0.557	5.75	0.532	5.67		
0.582	5.78	0.582	5.75	0.557	5.72		
				0.582	5.61		
				0.607	5.59		
				0.632	5.58		
P_0 = 84.4 psia		P_0 = 64.45 psia		P_0 = 24.45 psia		P_0 = 14.45 psia	
T_0 = 225° F		T_0 = 225° F		T_0 = 225° F		T_0 = 202° F	

Table 5

Summary of Hypersonic Laminar Boundary Layer Curvature Effects

M_1	d (inches)	δ^* (inches)	θ (inches)	θ/d	R_θ	C_f	$C_f/C_f^{\dagger}$ (flat plate)	
5.560	0.250	0.1767	0.0170	0.068	930	0.00150	3.32	GALCIT 5x5 inch Hypersonic Tunnel Measured Skin Friction
5.595	0.250	0.2040	0.0210	0.084	862	0.00230	4.76	
5.75	0.064	0.1267	0.0178	0.278	1102	-		
5.595	0.024	0.1422	0.0304	1.265	2000	-		

$\dagger$ C_f (flat plate) due to Van Driest (Ref. 15)

δ^* and θ are defined in Appendix B

Table 6

Summary of Hypersonic Turbulent Boundary Layer Curvature Effects

M_1	d (inches)	δ^* (inches)	θ (inches)	θ/d	R_θ	C_f	C_f/C_f (flat plate)†	
5.785	0.250	0.1355	0.0158	0.0540	2850	0.00185	1.45	GALCIT 5x5 inch Hypersonic Tunnel
5.775	0.250	0.1350	0.0162	0.0544	2540	0.00194	1.47	
5.760	0.250	0.1337	0.0152	0.0524	2140	0.00203	1.48	Measured Skin Friction
5.80	0.064	0.1461	0.0246	0.384	5170	0.00213	1.94	Estimated Skin Friction
5.825	0.024	0.1062	0.0210	0.875	4390	0.00234	2.04	Estimated Skin Friction

† C_f (flat plate) due to Korkegi (Ref. 16)

δ^* and θ are defined in Appendix B

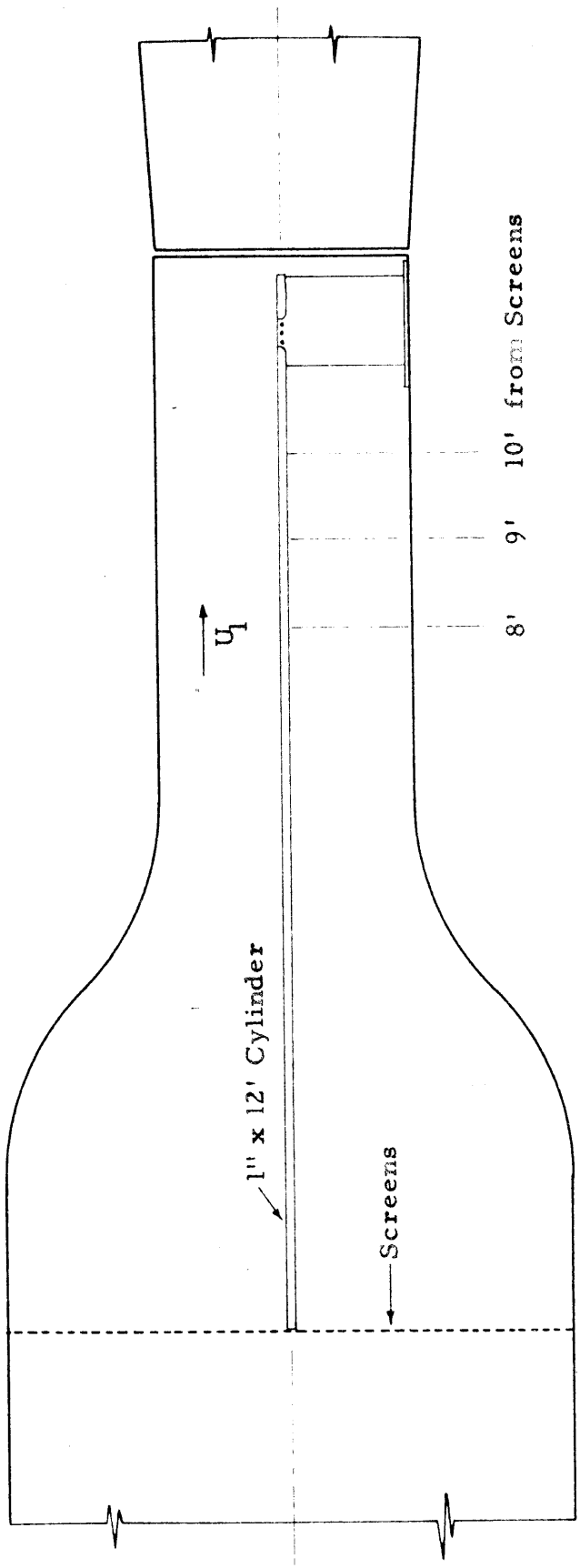

SCHEMATIC DIAGRAM OF 1" DIAMETER CYLINDER INSTALLATION IN THE MERRILL WIND TUNNEL

FIGURE 1

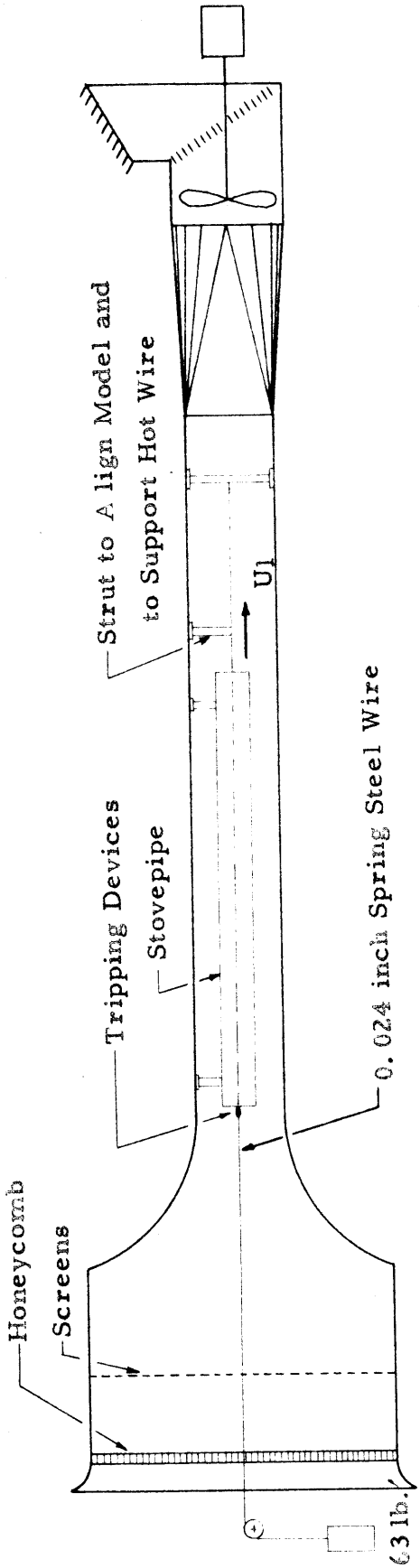

SCHEMATIC DIAGRAM OF THE 0.024 INCH WIRE MODEL INSTALLATION
IN THE LOW TURBULENCE TUNNEL

FIGURE 3

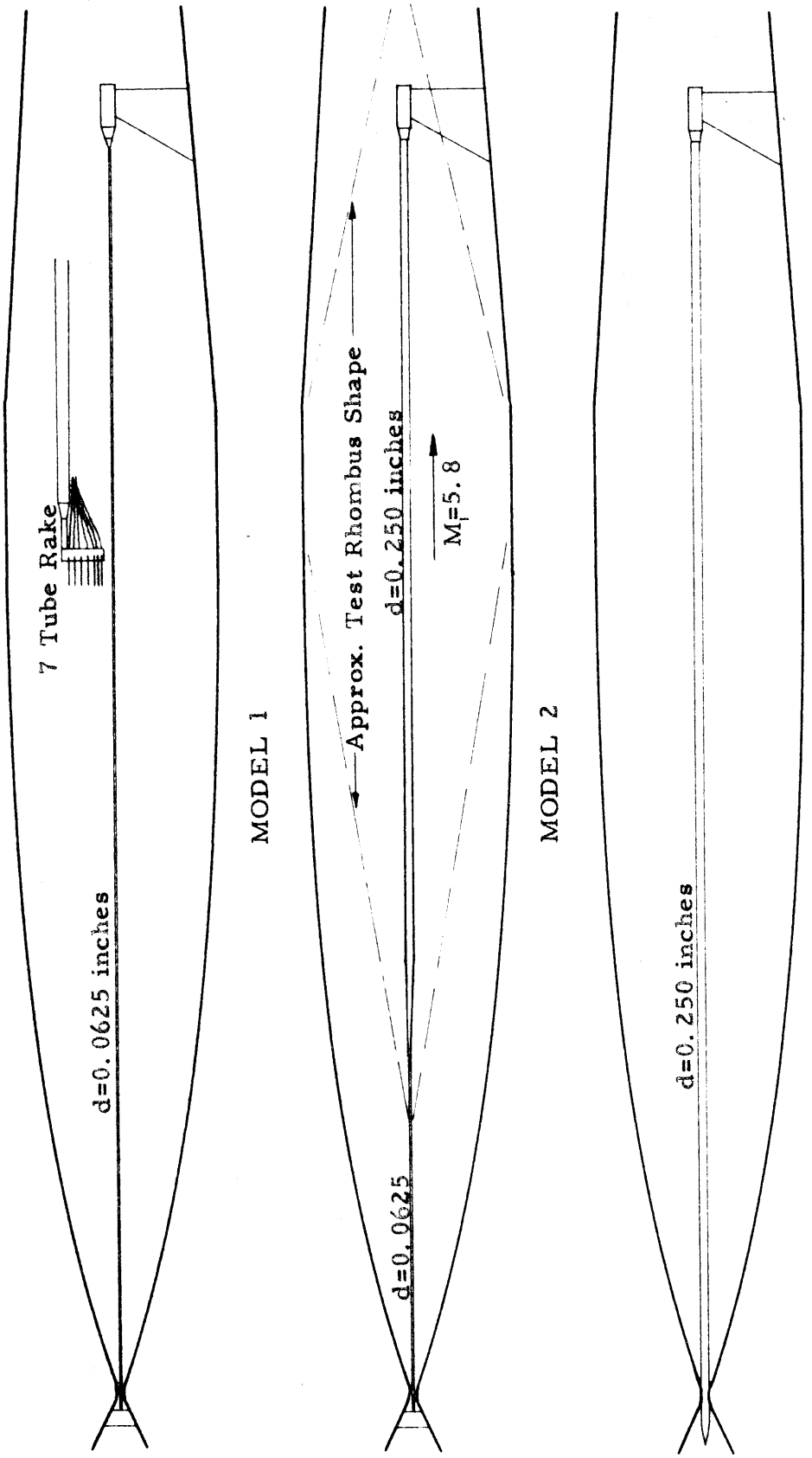

SCHEMATIC DIAGRAM OF CYLINDER MODELS IN THE 5x5 INCH HYPERSONIC TUNNEL

FIGURE 3

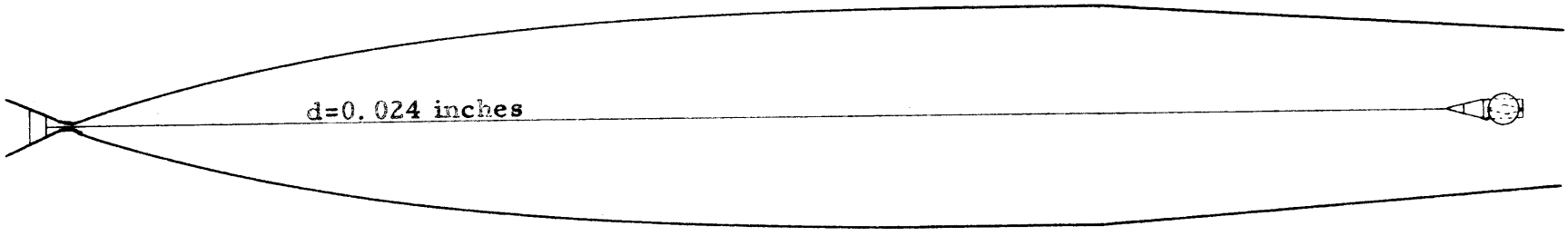

MODEL 4

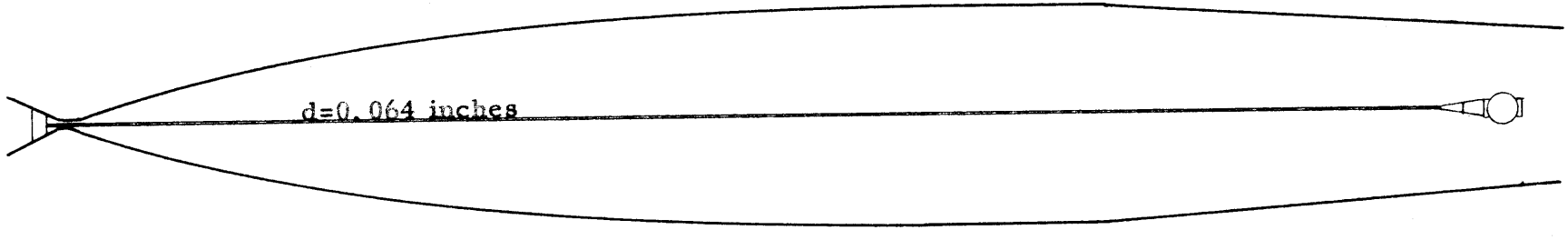

MODEL 5

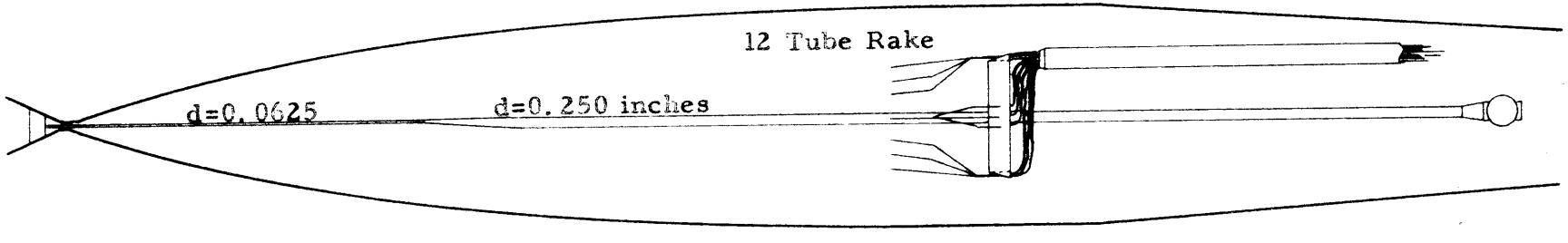

MODEL 6

SCHEMATIC DIAGRAM OF CYLINDER MODELS IN THE 5x5 INCH HYPERSONIC TUNNEL

FIGURE 4

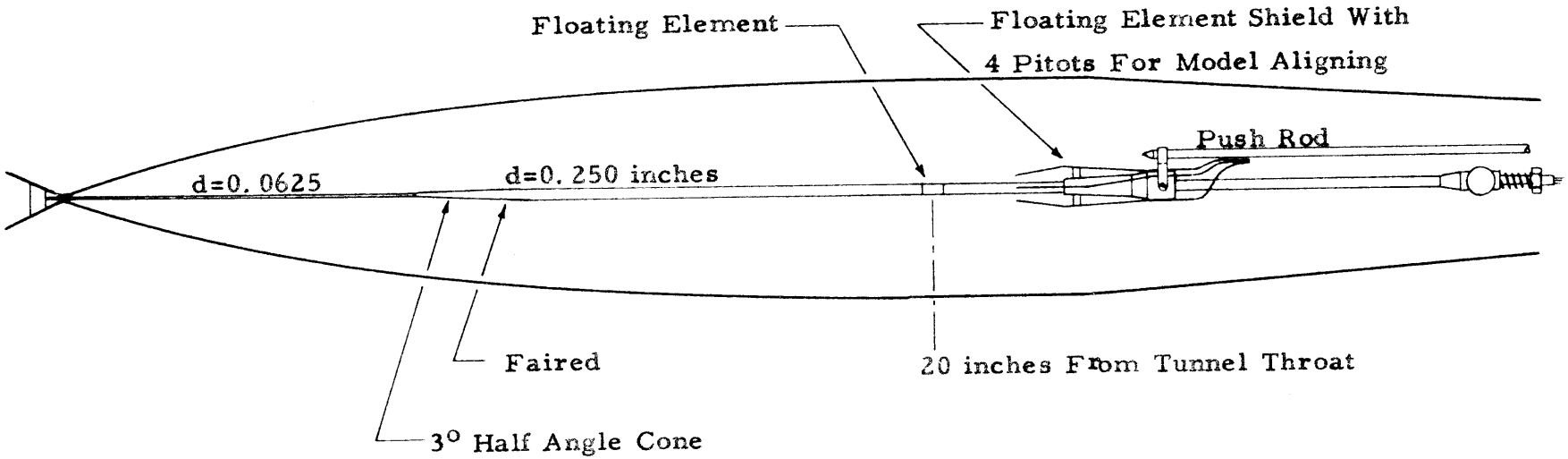

SCHEMATIC DIAGRAM OF THE 0.250 INCH SKIN FRICTION MODEL AND STARTING SHIELD IN THE 5x5 INCH HYPERSONIC TUNNEL

FIGURE 5

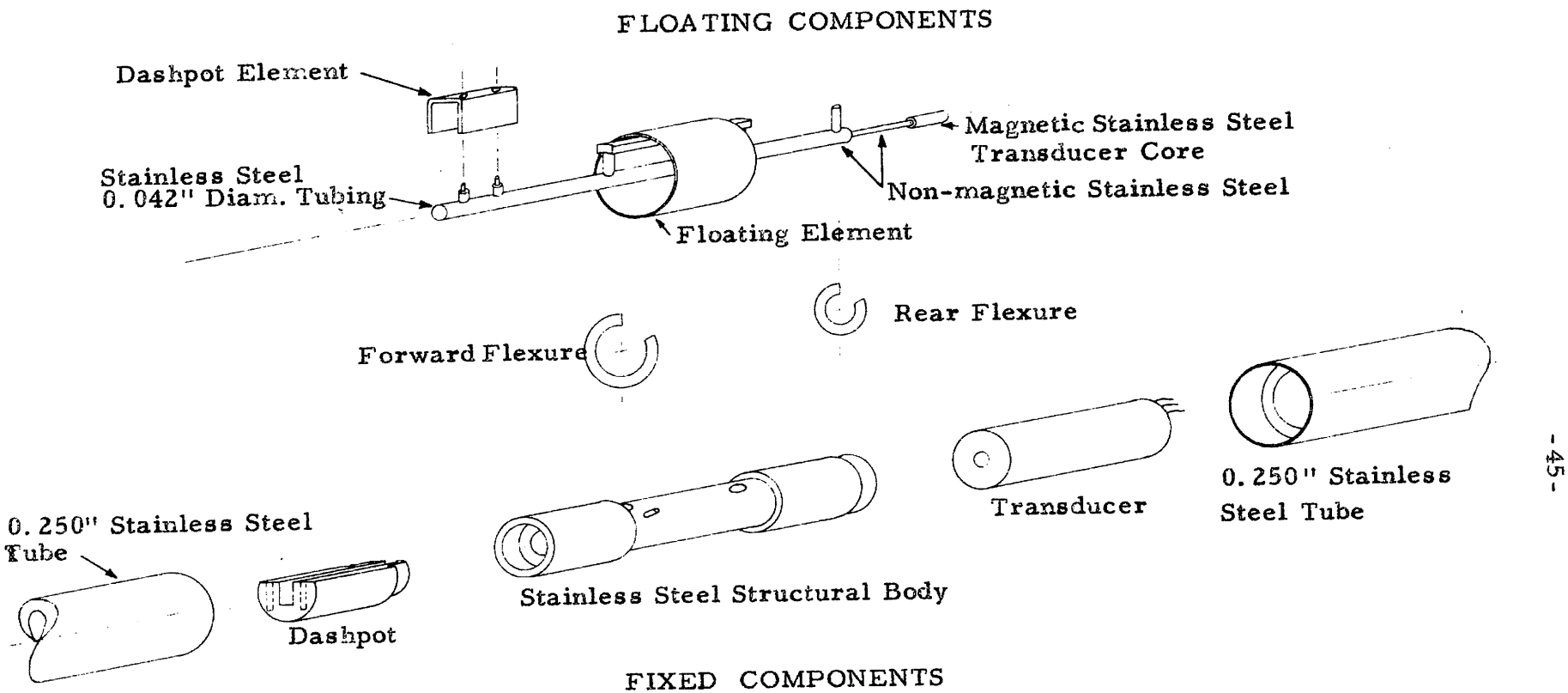

CABINET DRAWING OF THE 0.250 INCH SKIN FRICTION MODEL FLOATING ELEMENT MECHANISM

FIGURE 6

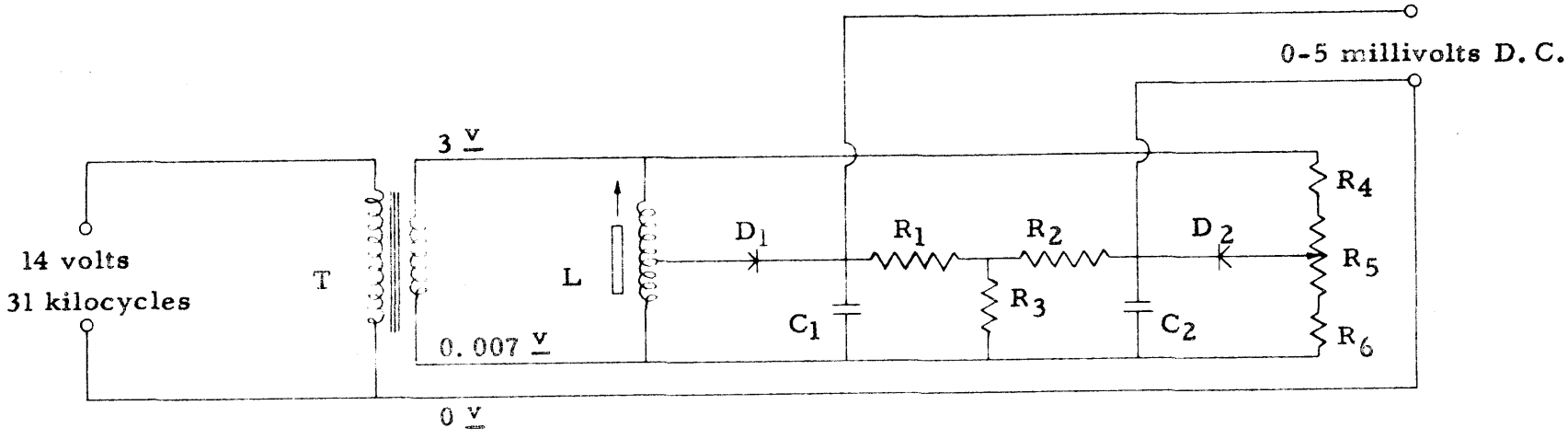

SPECIFICATIONS:

T= General Radio Shielded Transformer
L= Crescent Engineering "Transducer"
D_1, D_2= 1N34A Sylvania Germanium Diodes
C_1, C_2= 0.25 Microfarads
R_1; R_2= 2000 Ohms
R_3= 14000 Ohms
R_4= 300 Ohms
R_5= 200 Ohm Ten Turn Helipot
R_6= 500 Ohms

ELECTRIC CIRCUIT FOR THE SKIN FRICTION METER

FIGURE 7

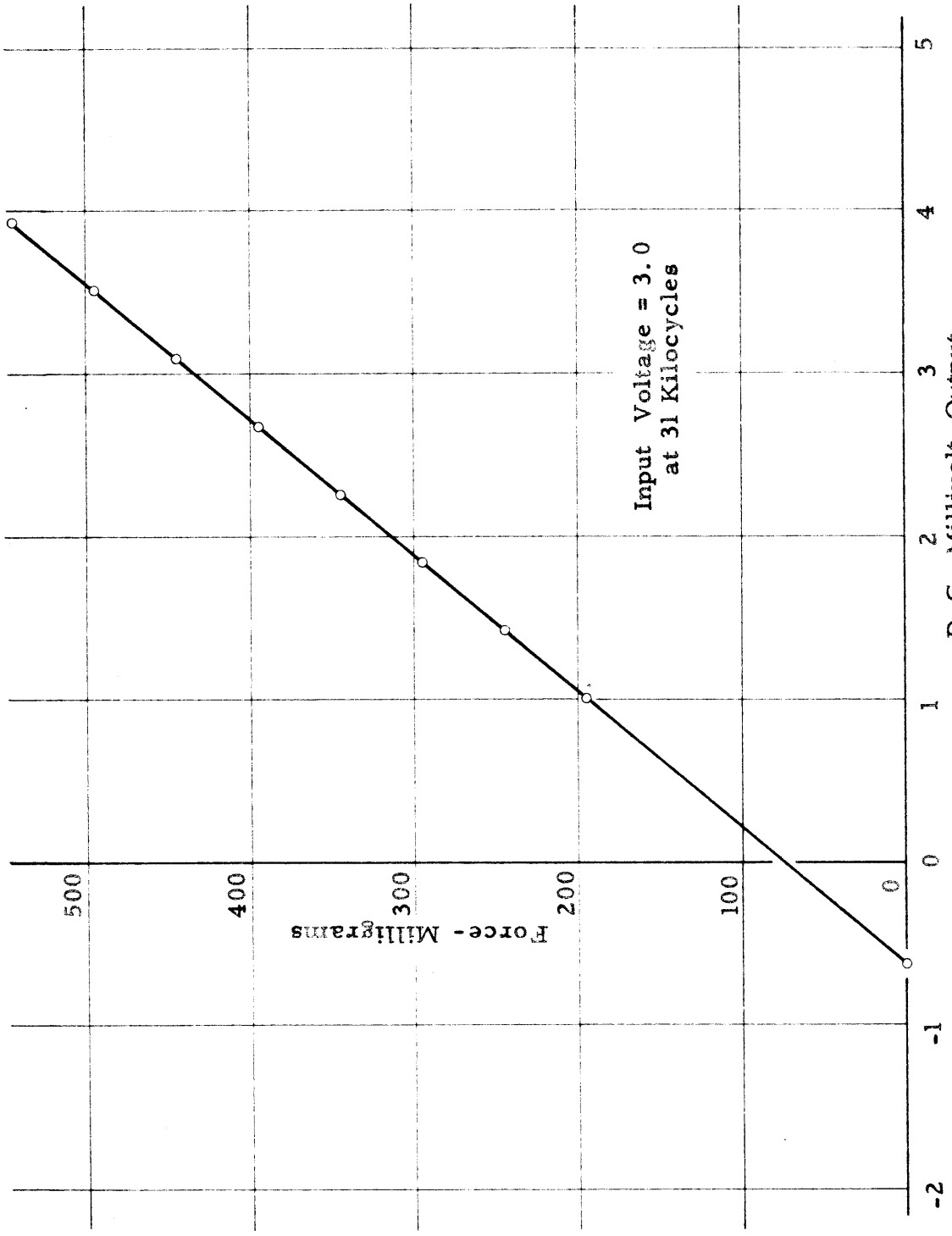

TYPICAL CALIBRATION OF THE SKIN FRICTION METER

FIGURE 8

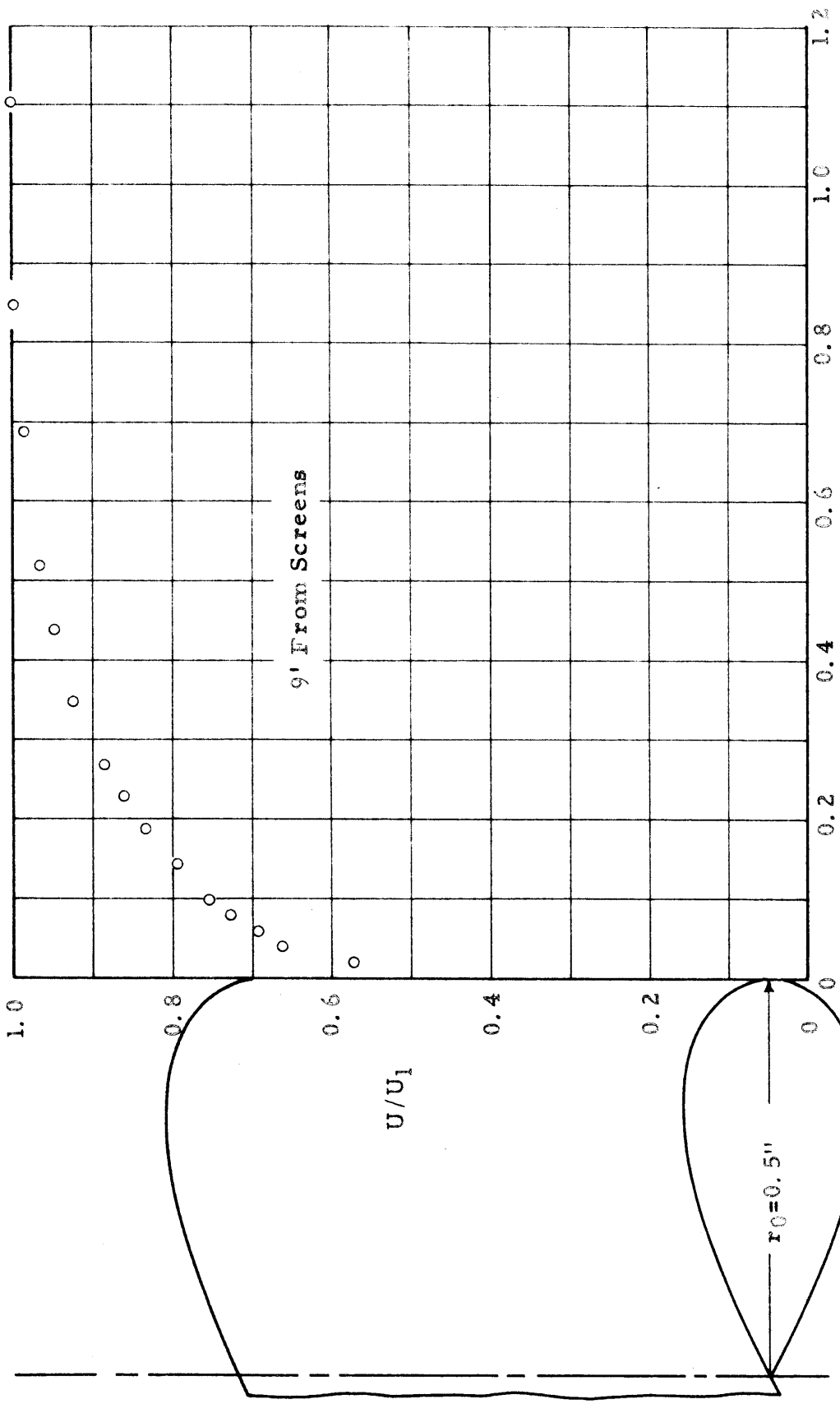

TURBULENT BOUNDARY LAYER PROFILE WITH AXIAL FLOW ON A 1 INCH DIAMETER CYLINDER IN THE MERRILL WIND TUNNEL

FIGURE 9a

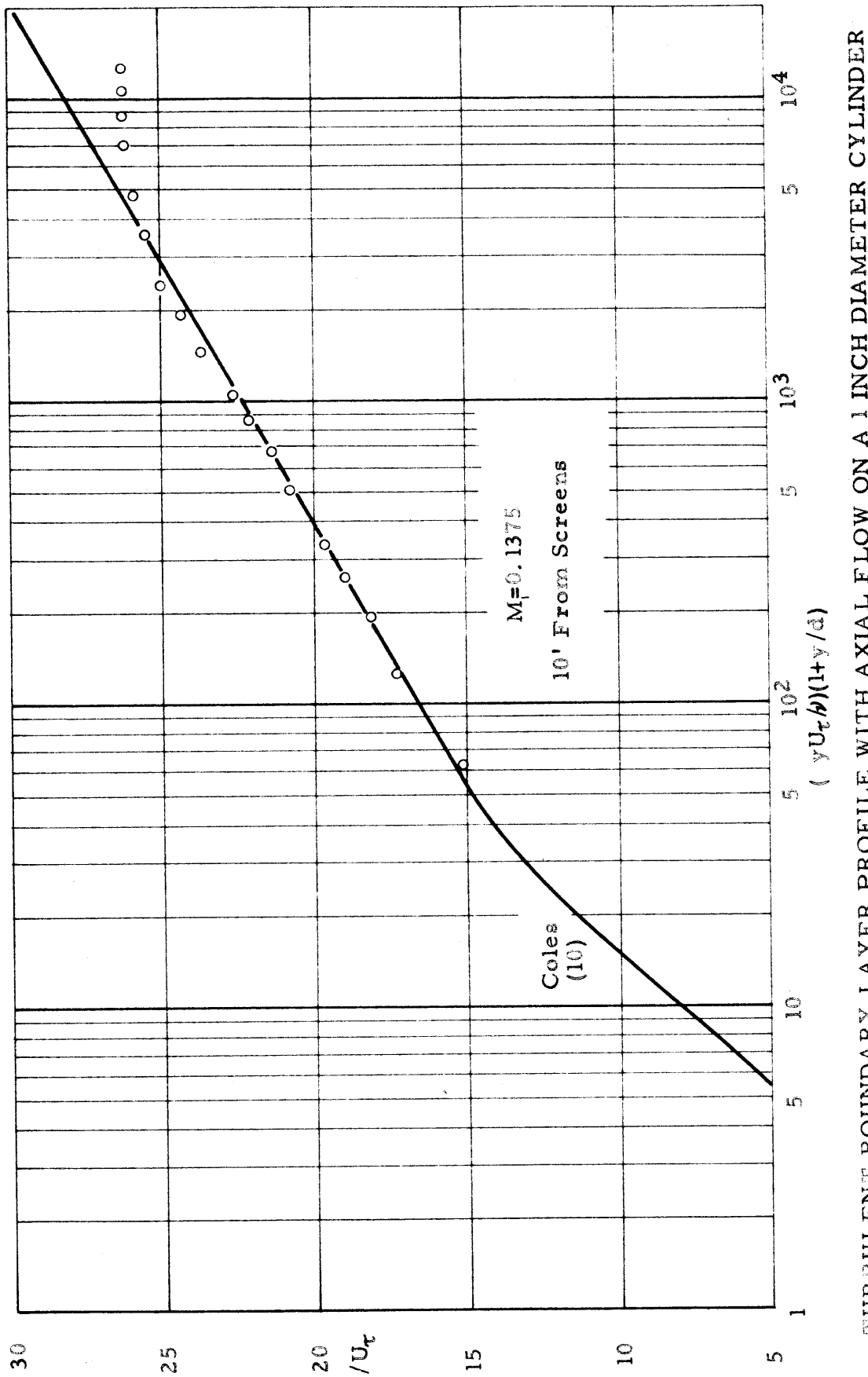

TURBULENT BOUNDARY LAYER PROFILE WITH AXIAL FLOW ON A 1 INCH DIAMETER CYLINDER IN THE MERRILL WIND TUNNEL

FIGURE 9b

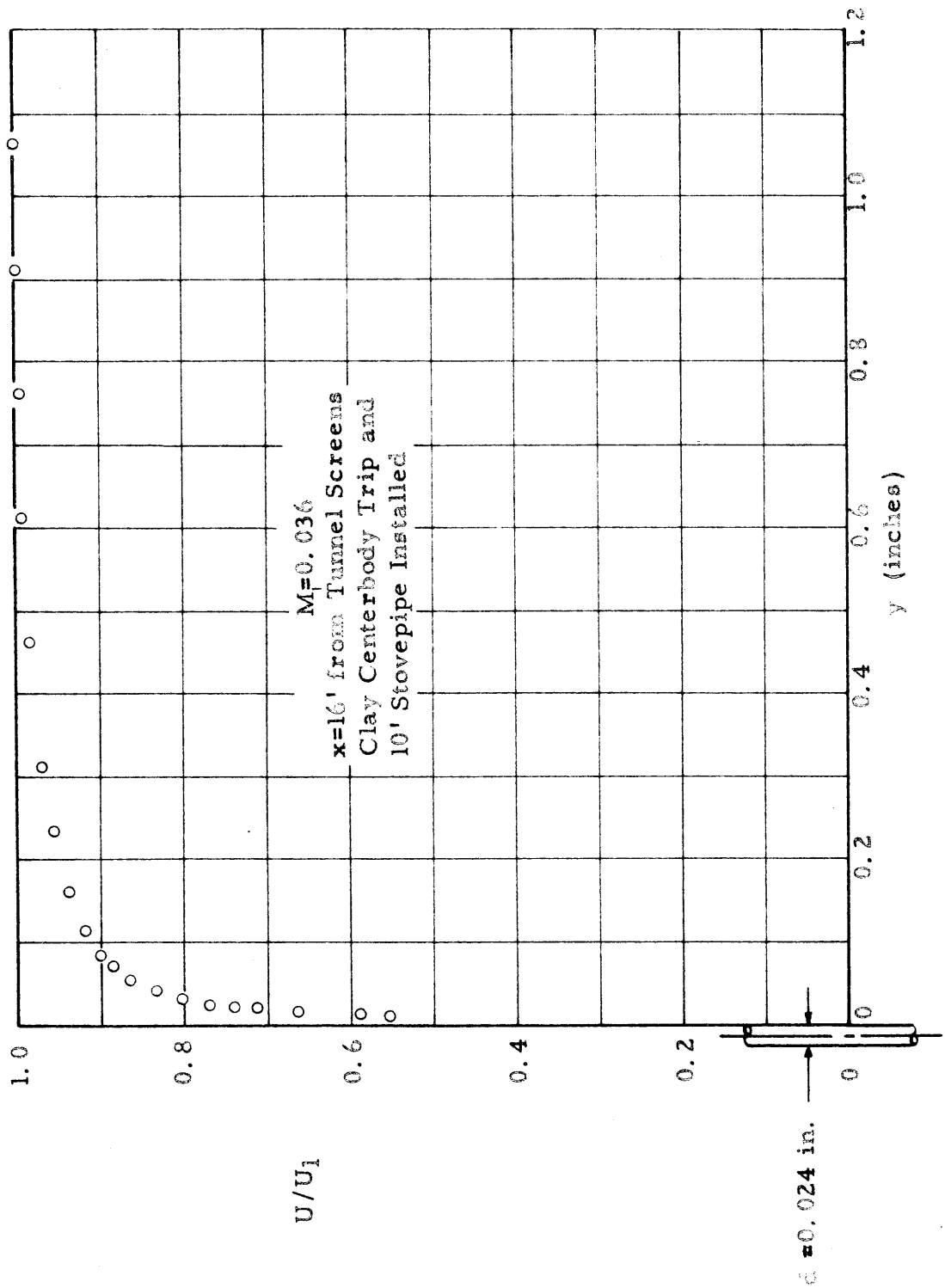

TURBULENT BOUNDARY LAYER PROFILE WITH AXIAL FLOW ON A 0.024 INCH DIAM. CYLINDER IN THE LOW TURBULENCE WIND TUNNEL

FIGURE 10a

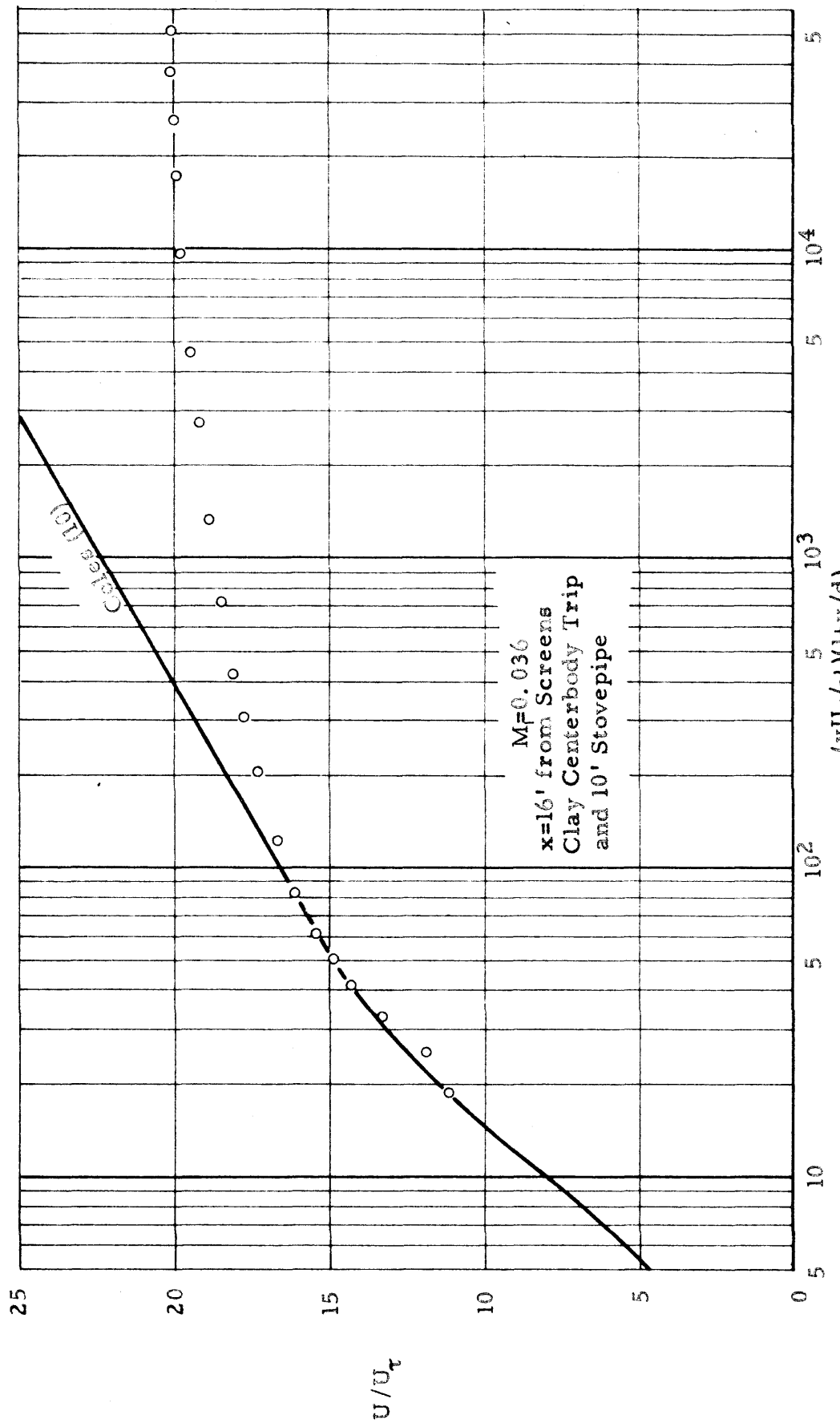

TURBULENT BOUNDARY LAYER PROFILE WITH AXIAL FLOW ON A 0.024 INCH DIAM. CYLINDER IN THE LOW TURBULENCE WIND TUNNEL

FIGURE 10b

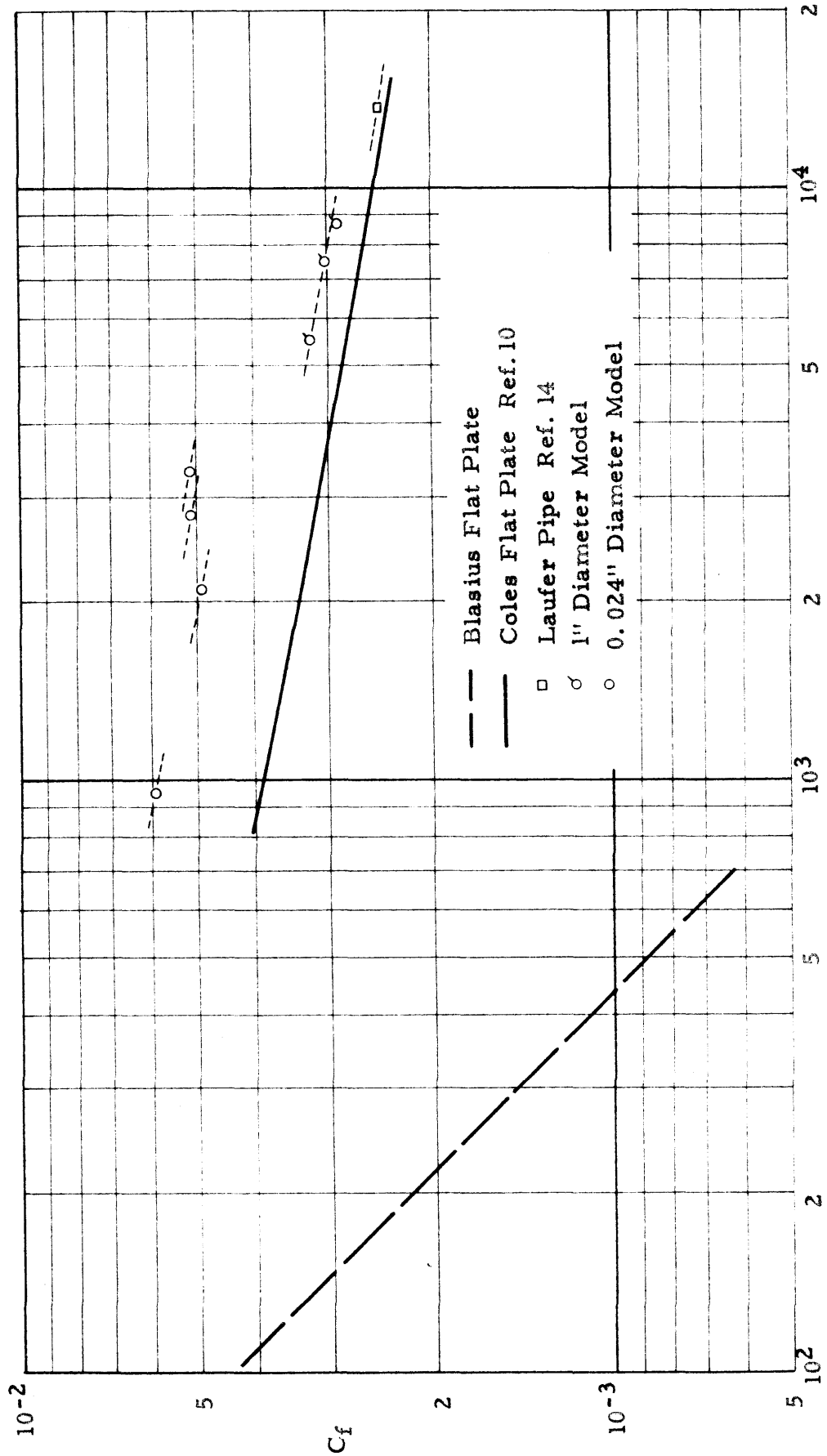

SUBSONIC TURBULENT BOUNDARY LAYER ESTIMATED SKIN FRICTION

FIGURE 11

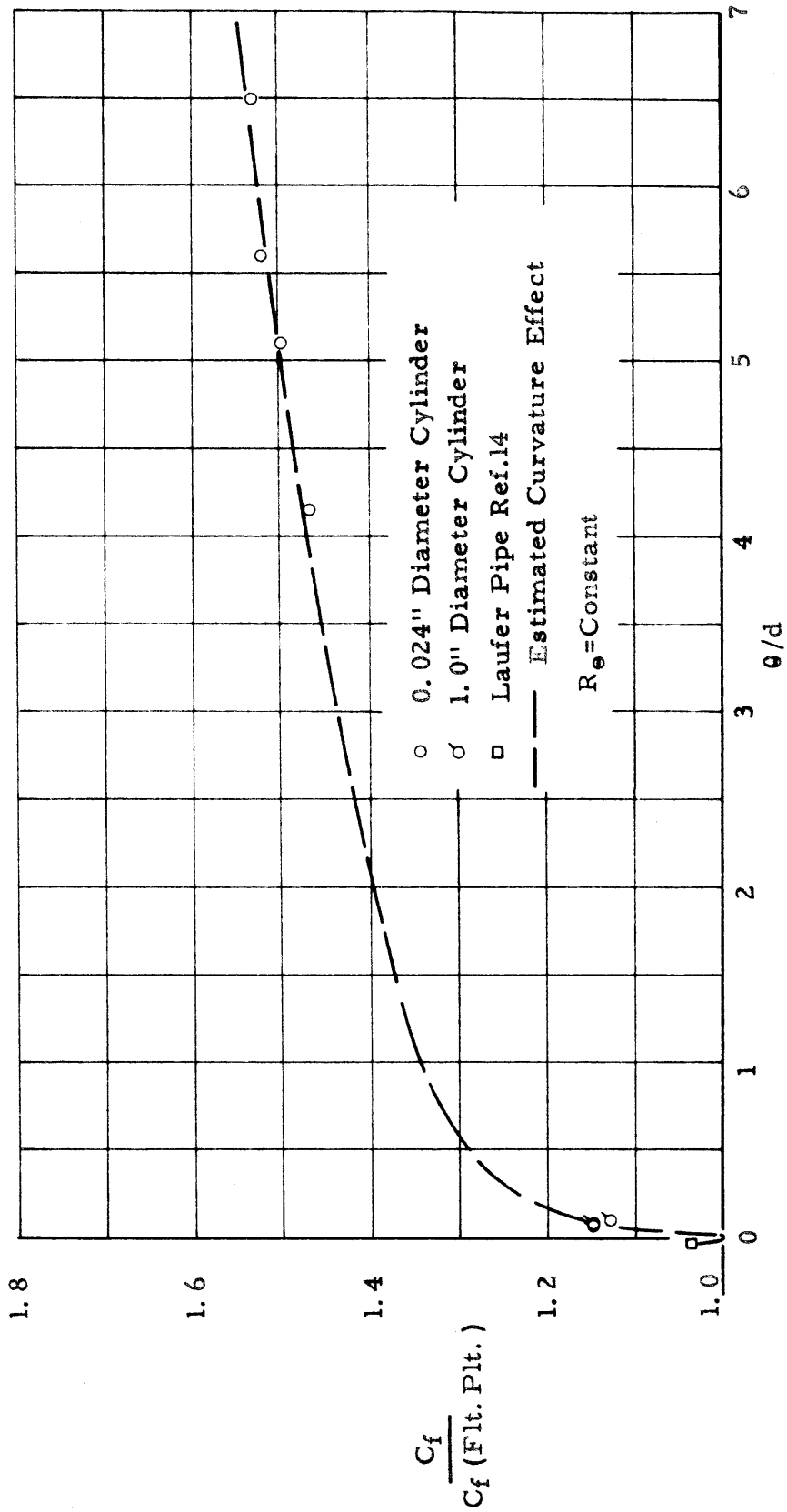

RATIO OF TURBULENT SKIN FRICTION ON A CYLINDER TO THAT ON A FLAT PLATE AT SUBSONIC SPEEDS

FIGURE 12

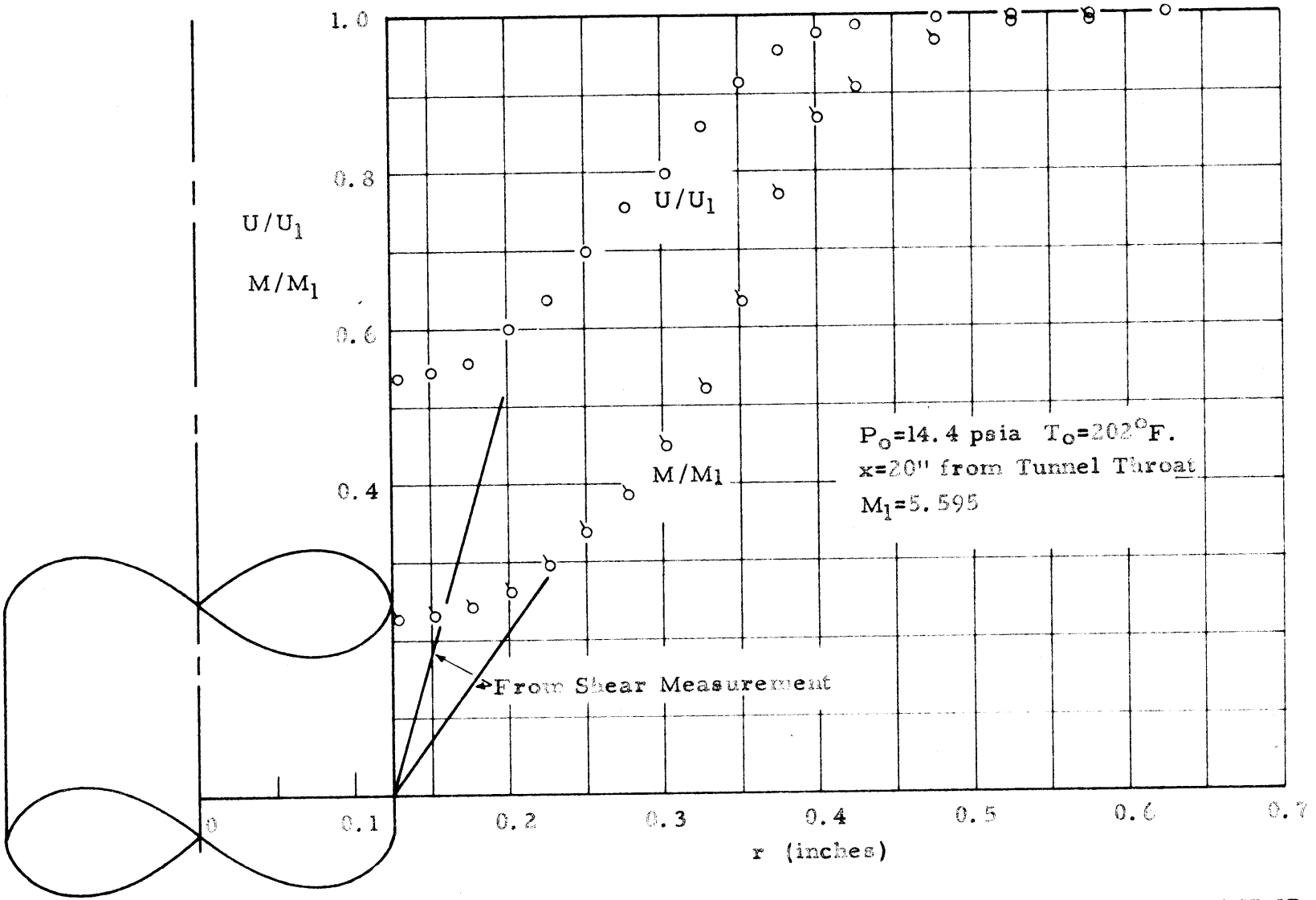

LAMINAR BOUNDARY LAYER PROFILE WITH AXIAL FLOW ON A 0.250 INCH DIAM. CYLINDER IN THE 5x5 INCH HYPERSONIC WIND TUNNEL

FIGURE 13

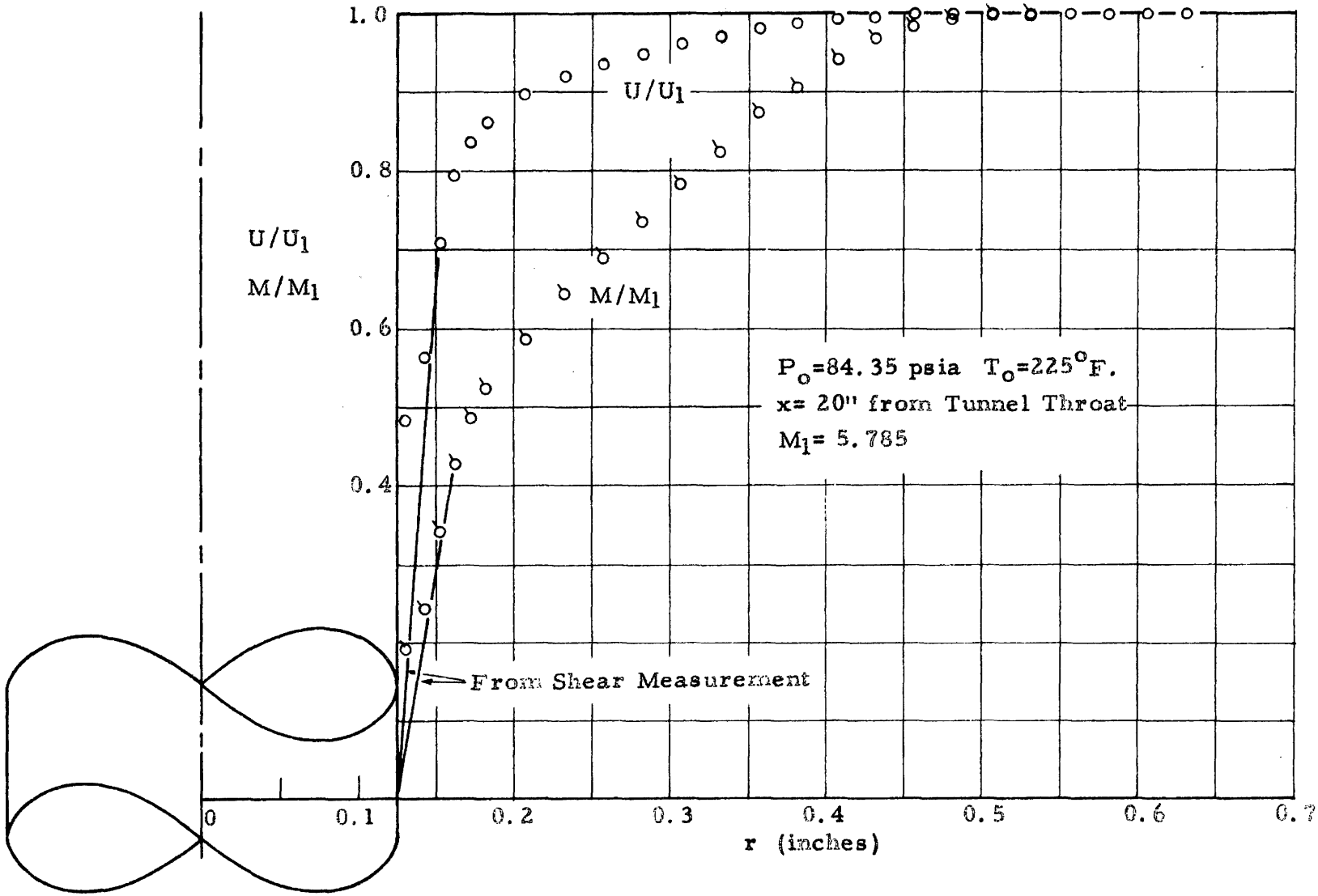

TURBULENT BOUNDARY LAYER PROFILE WITH AXIAL FLOW ON A 0.250 INCH DIAM. CYLINDER IN THE 5x5 INCH HYPERSONIC WIND TUNNEL
FIGURE 14a

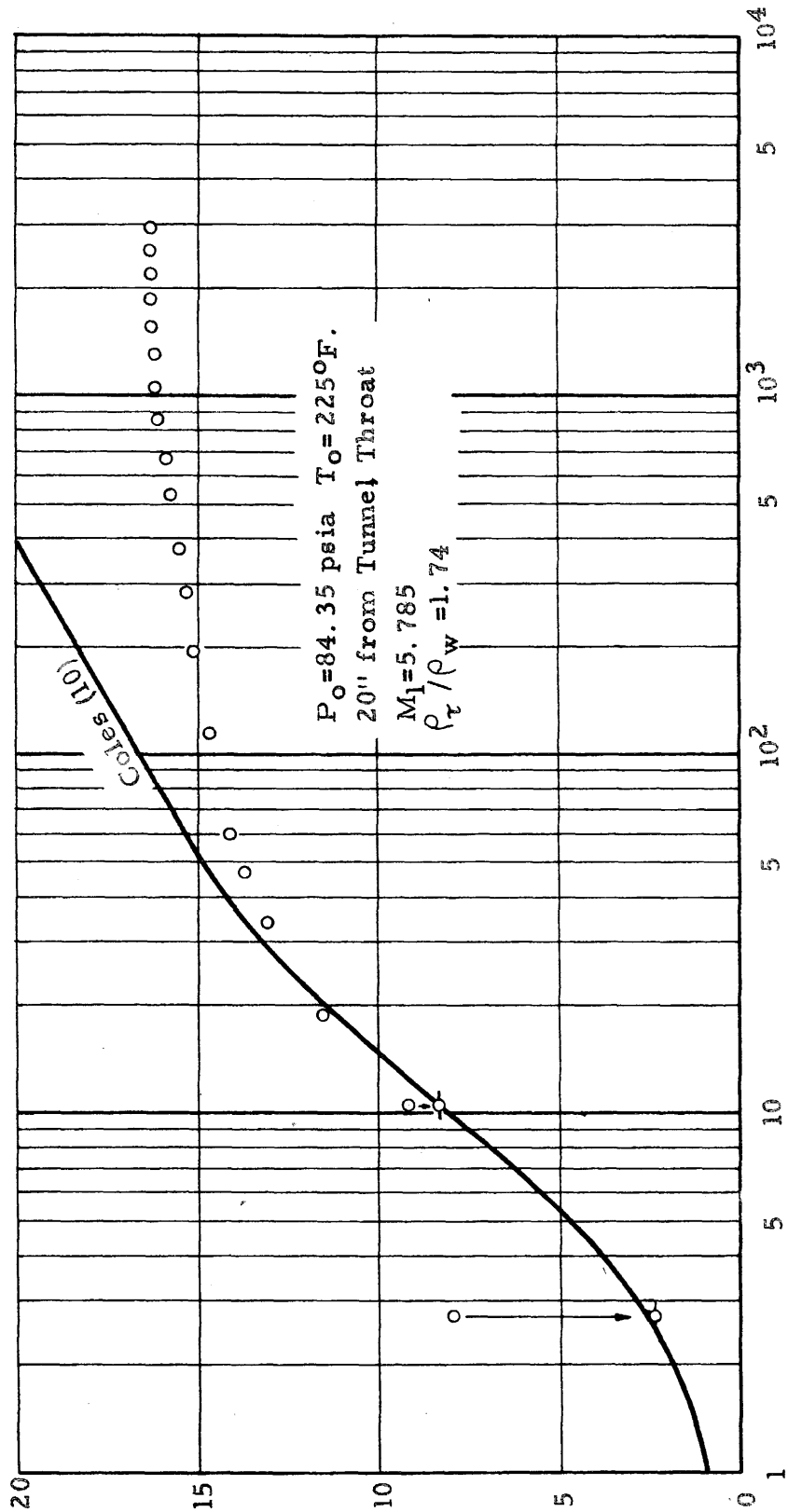

TURBULENT BOUNDARY LAYER PROFILE WITH AXIAL FLOW ON A 0.250 INCH DIAM. CYLINDER IN THE 5x5 INCH HYPERSONIC WIND TUNNEL

FIGURE 14b

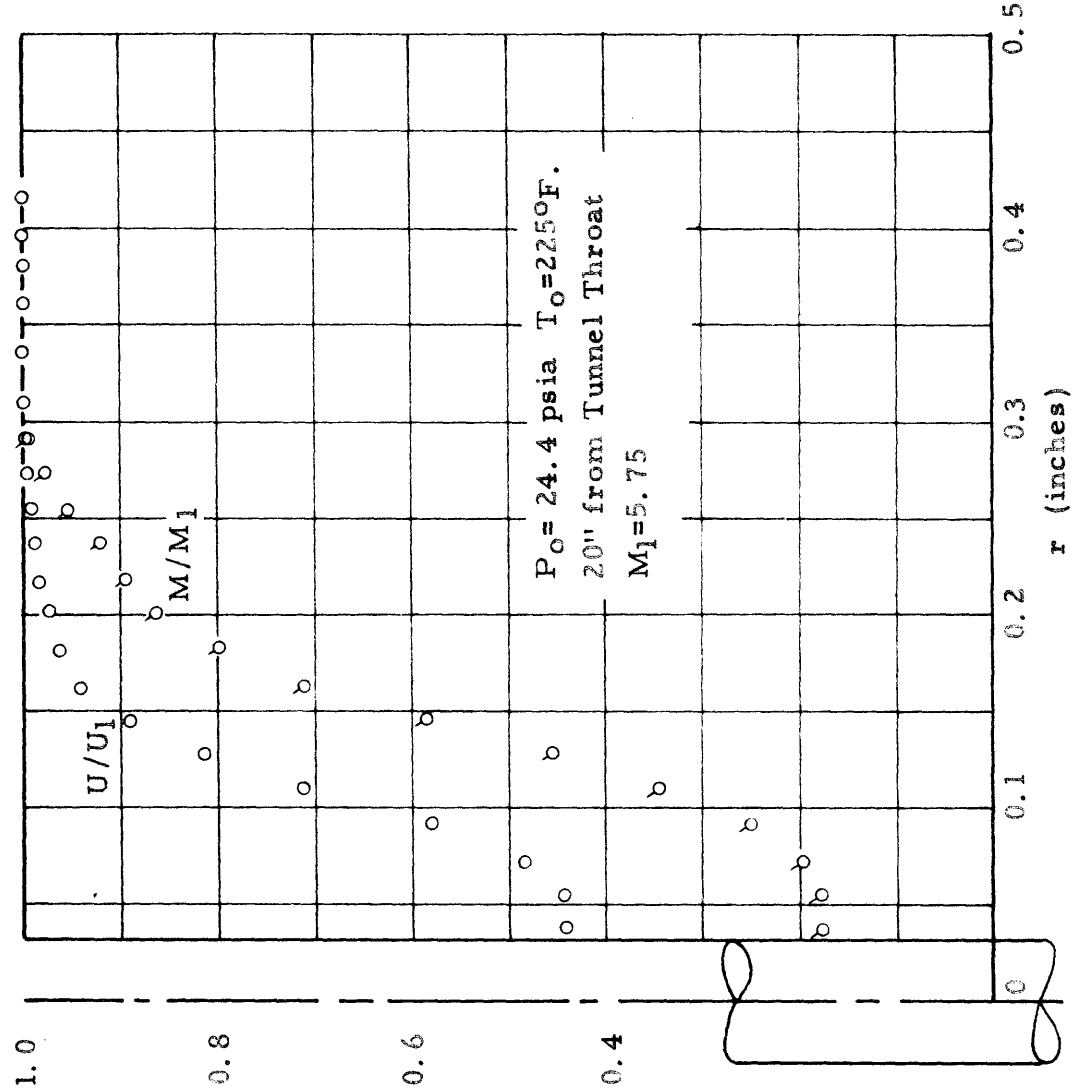

LAMINAR BOUNDARY LAYER PROFILE WITH AXIAL FLOW ON A 0.064 INCH DIAM. CYLINDER IN THE 5x5 INCH HYPERSONIC WIND TUNNEL

FIGURE 15

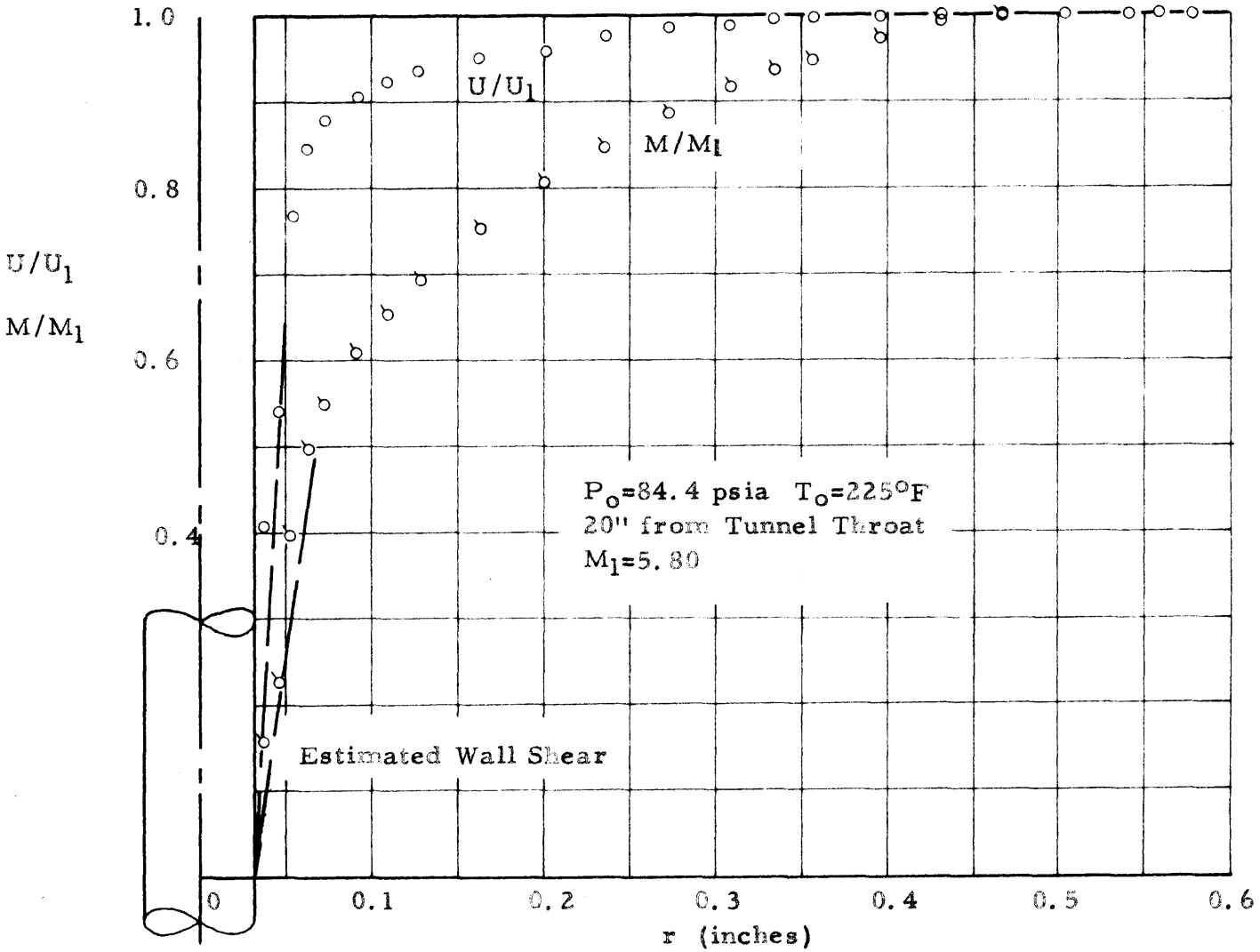

TURBULENT BOUNDARY LAYER PROFILE WITH AXIAL FLOW ON A 0.064 INCH DIAM. CYLINDER IN THE 5x5 INCH HYPERSONIC WIND TUNNEL

FIGURE 16a

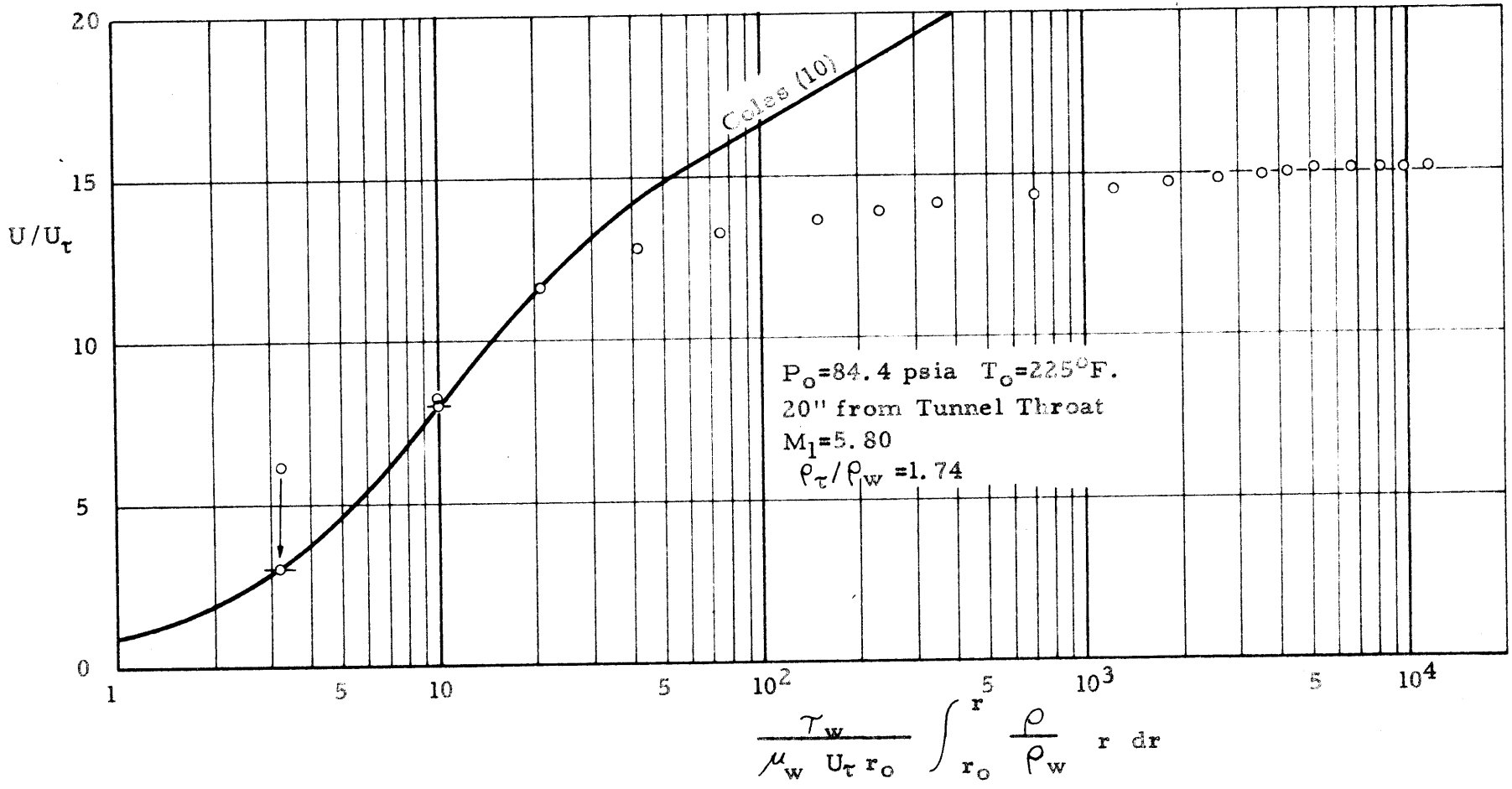

TURBULENT BOUNDARY LAYER PROFILE WITH AXIAL FLOW ON A 0.064 INCH DIAM. CYLINDER IN THE 5x5 INCH HYPERSONIC WIND TUNNEL

FIGURE 16b

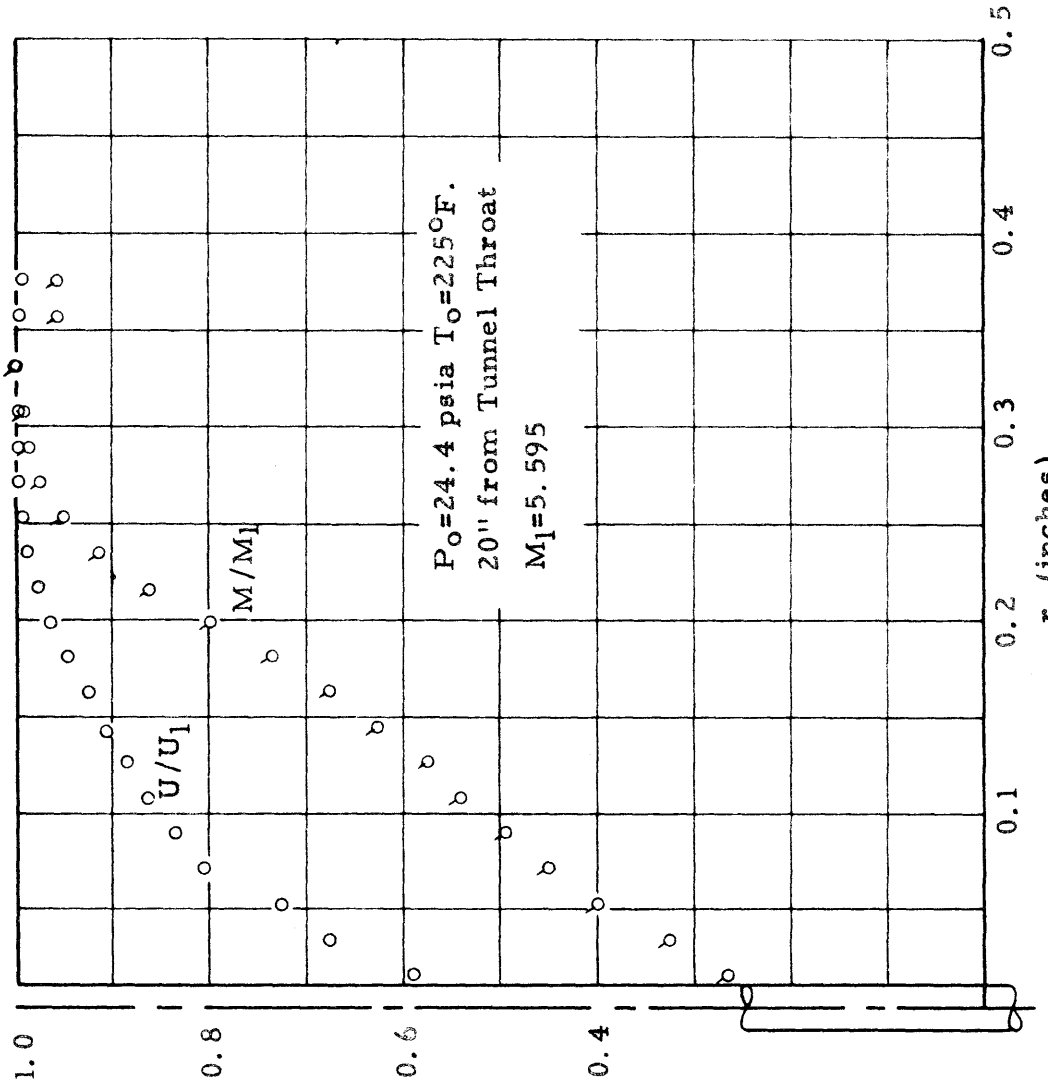

LAMINAR BOUNDARY LAYER PROFILE WITH AXIAL FLOW ON A 0.024 INCH DIAM. CYLINDER IN THE 5x5 INCH HYPERSONIC WIND TUNNEL

FIGURE 17

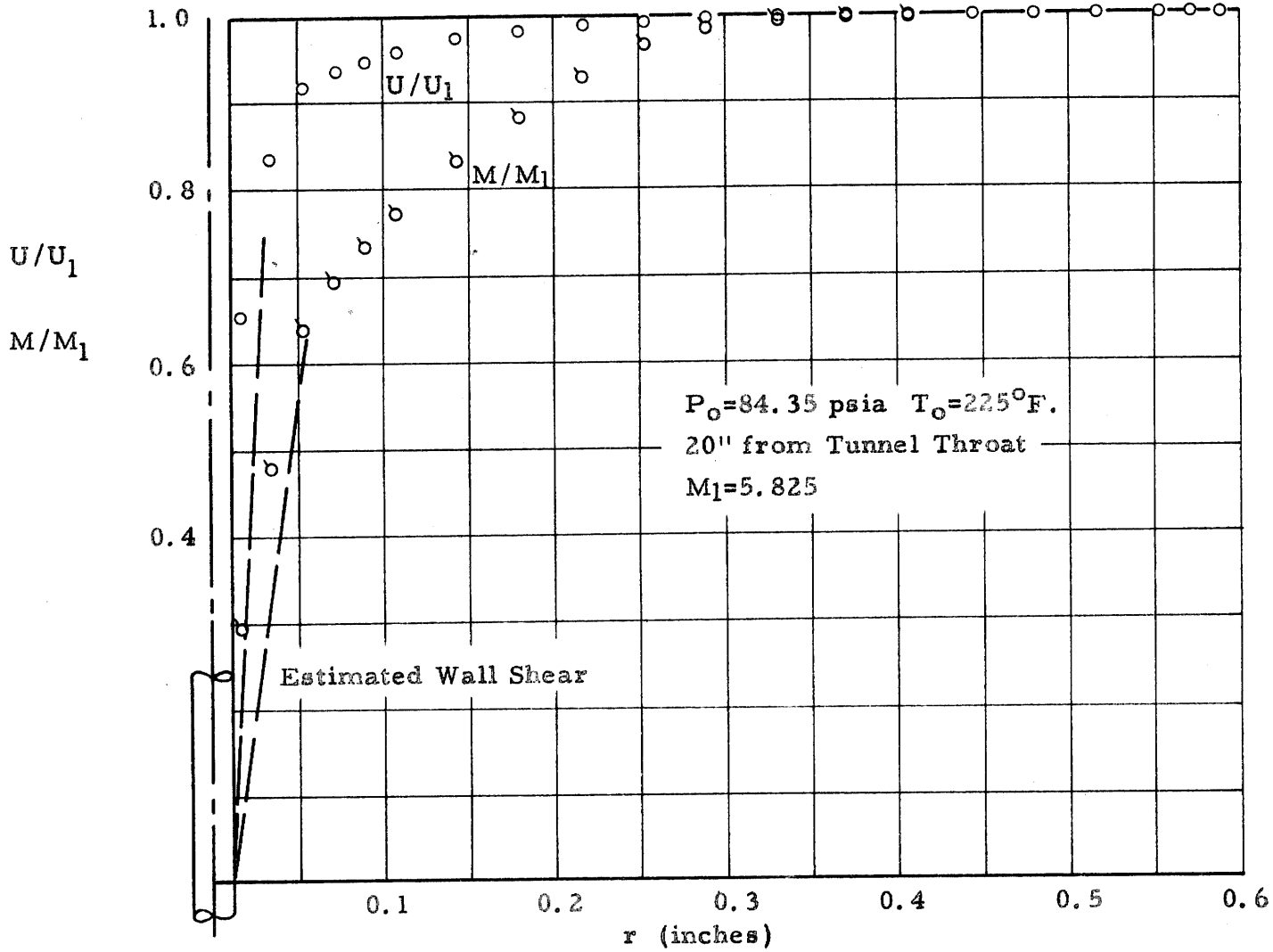

TURBULENT BOUNDARY LAYER PROFILE WITH AXIAL FLOW ON A 0.024 INCH DIAM. CYLINDER IN THE 5x5 INCH HYPERSONIC WIND TUNNEL

FIGURE 18a

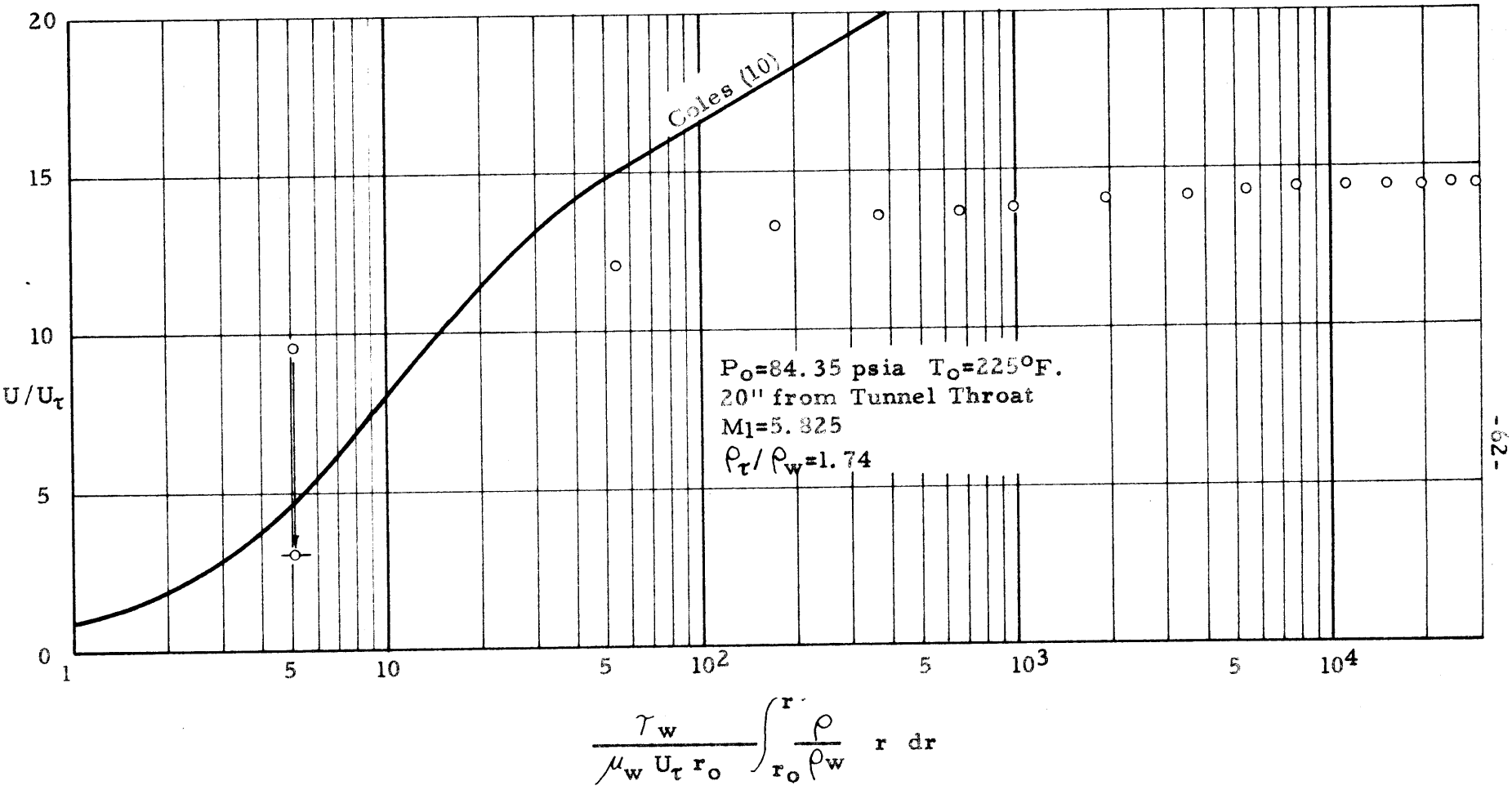

TURBULENT BOUNDARY LAYER PROFILE WITH AXIAL FLOW ON A 0.024 INCH DIAM. CYLINDER IN THE 5x5 INCH HYPERSONIC WIND TUNNEL

FIGURE 18b

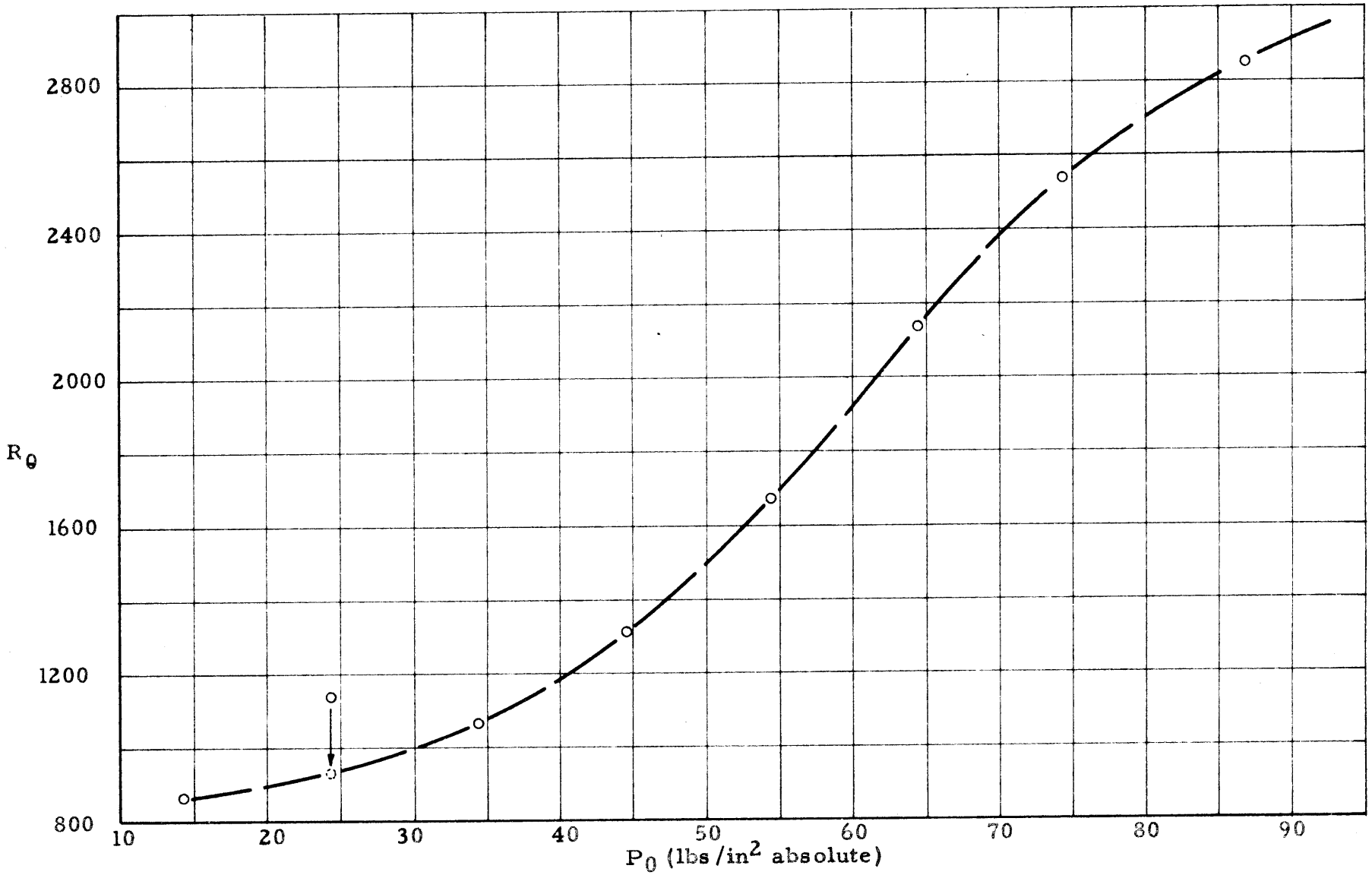

COMPUTED MOMENTUM THICKNESS REYNOLDS NUMBER ON THE 0.250 INCH SKIN FRICTION MODEL

FIGURE 19

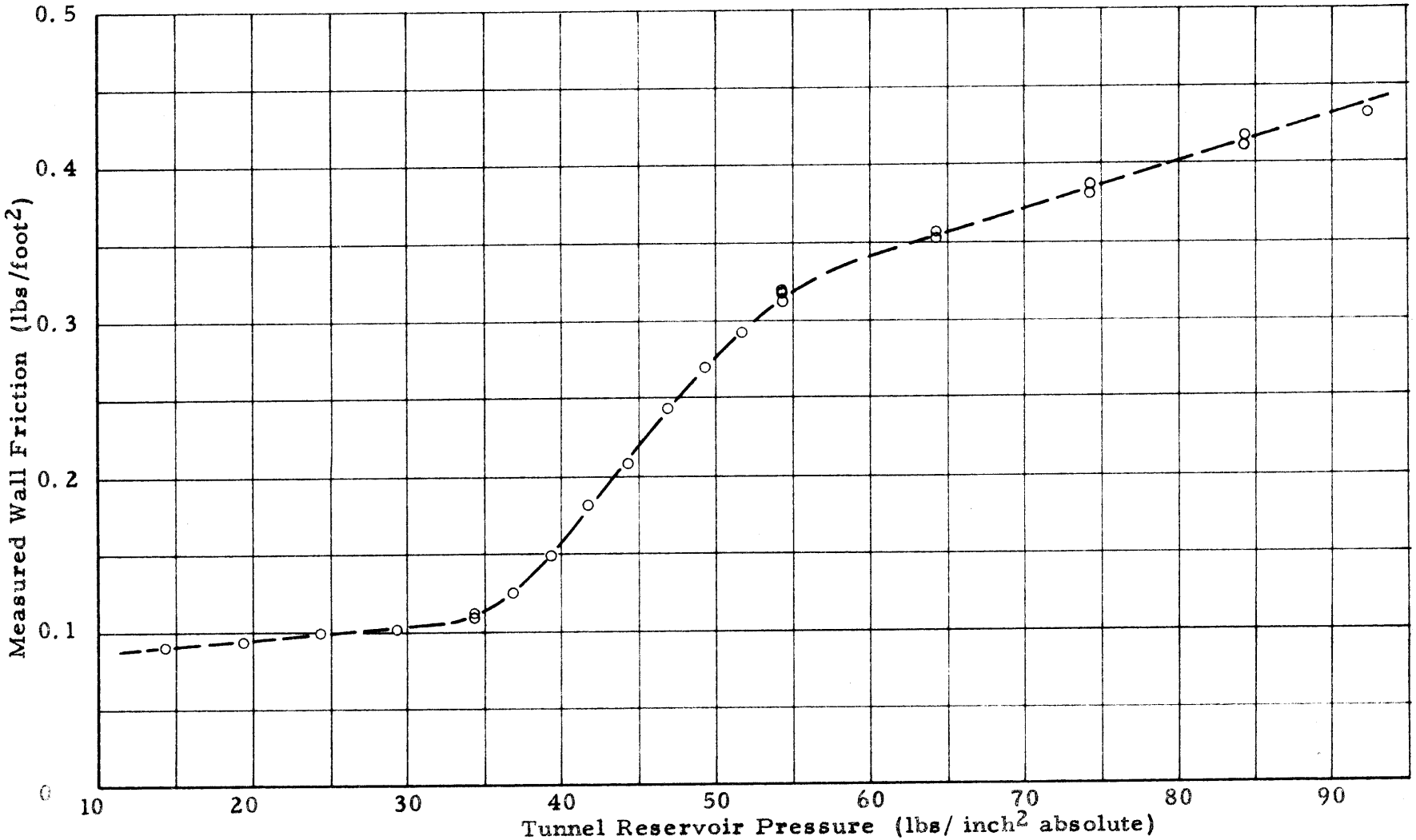

MEASURED SKIN FRICTION ON THE 0.250 INCH MODEL VERSES TUNNEL RESERVOIR PRESSURE

FIGURE 20

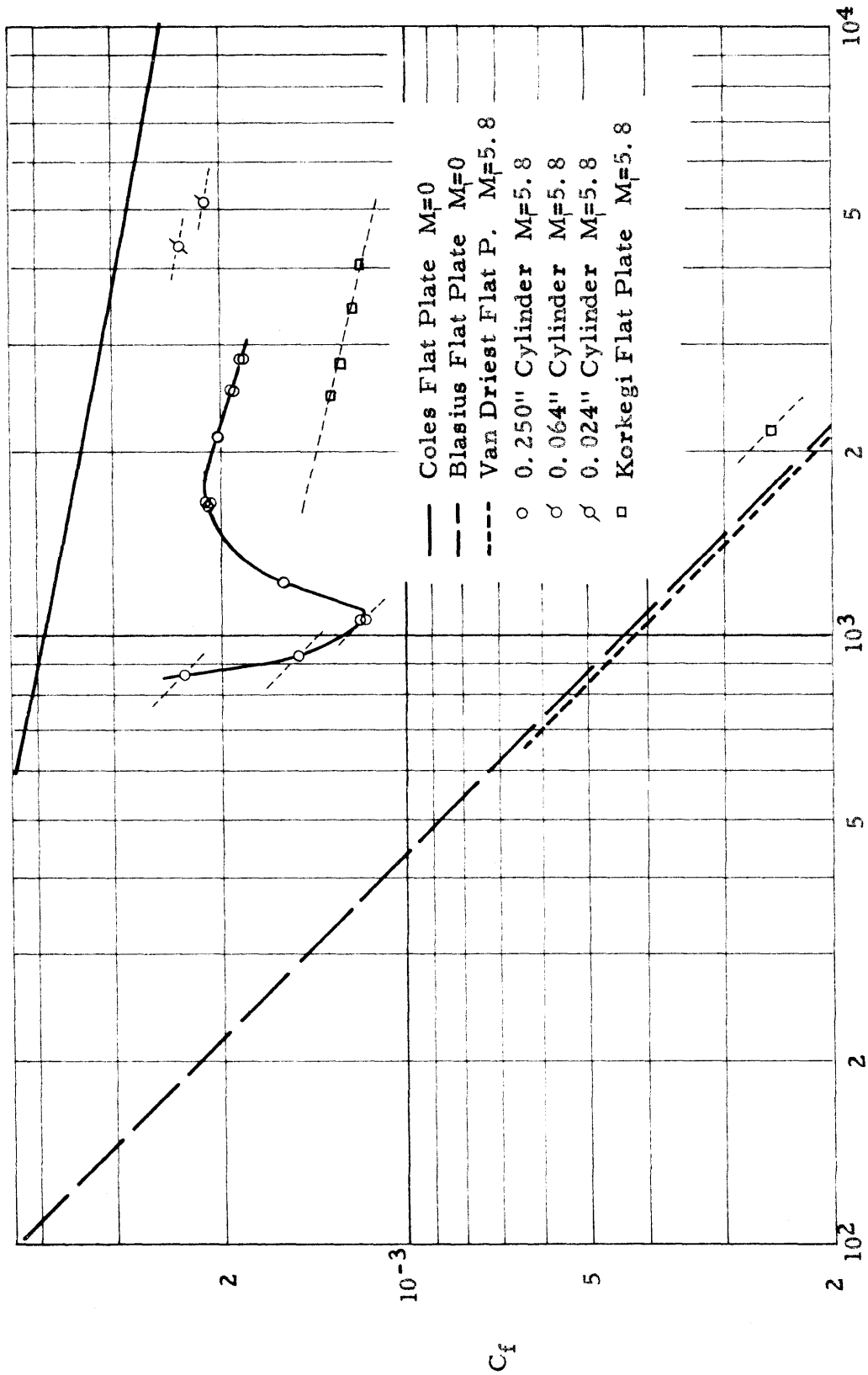

HYPERSONIC LAMINAR AND TURBULENT BOUNDARY LAYER SKIN FRICTION

FIGURE 21

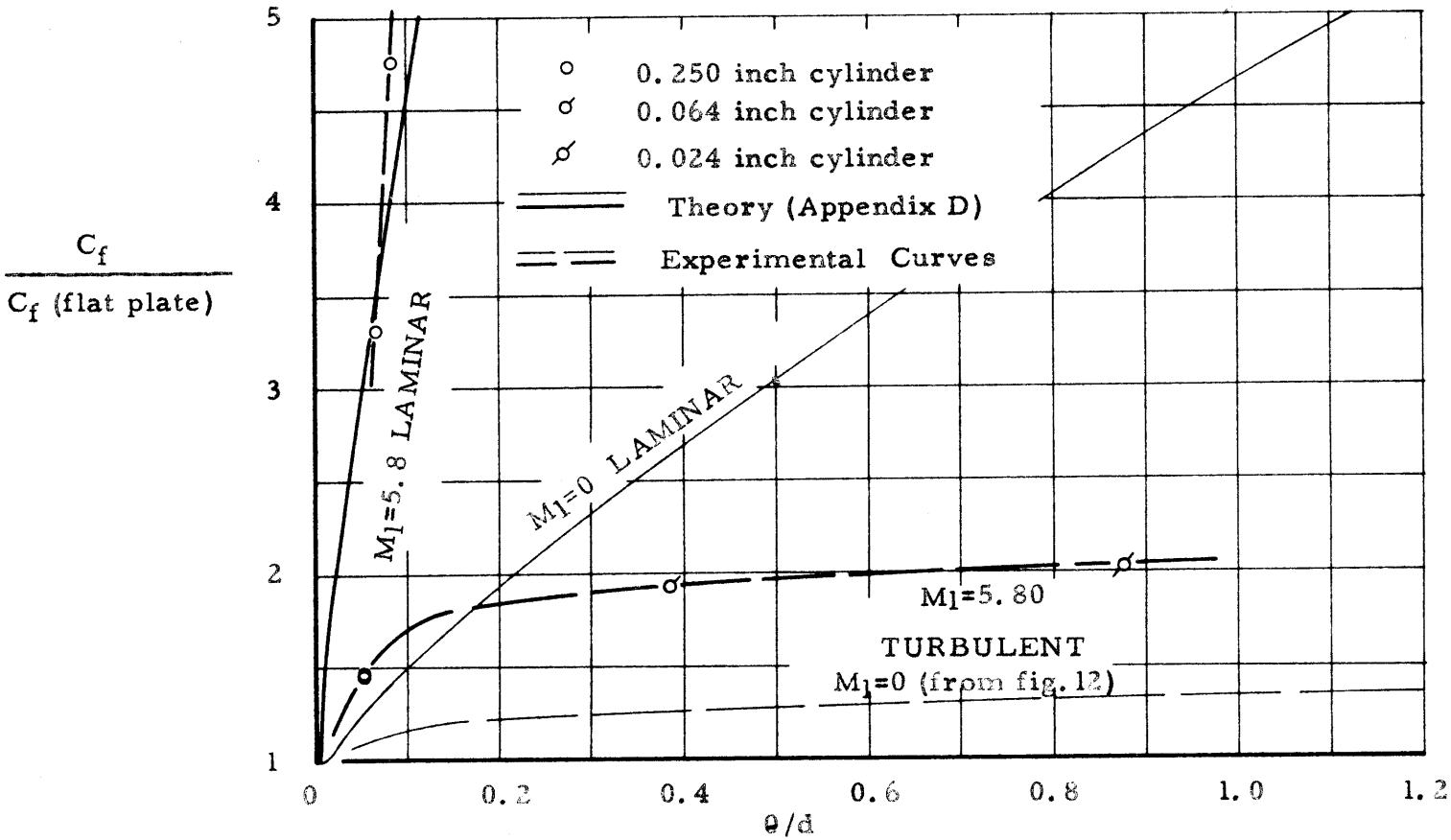

RATIO OF SKIN FRICTION ON A CYLINDER TO THAT ON A FLAT PLATE AT M=0 and M=5.8 AT CONSTANT R_θ

FIGURE 22